

# Cluster Ages to Reconstruct the Milky Way Assembly (CARMA)

## II. The age-metallicity relation of Gaia-Sausage-Enceladus globular clusters.

Fernando Aguado-Agelet<sup>1,2</sup>, Davide Massari<sup>3</sup>, Matteo Monelli<sup>4,5</sup>, Santi Cassisi<sup>5,6</sup>, Carme Gallart<sup>7</sup>, Edoardo Ceccarelli<sup>3,8</sup>, Yllari Kay González Koda<sup>9</sup>, Tomás Ruiz-Lara<sup>9</sup>, Elena Pancino<sup>10</sup>, Sara Saracino<sup>10,11</sup>, Maurizio Salaris<sup>11</sup>

<sup>1</sup> atlanTTic, Universidade de Vigo, Escola de Enxeñaría de Telecomunicación, 36310, Vigo, Spain  
e-mail: faguado@uvigo.gal

<sup>2</sup> Universidad de La Laguna, Avda. Astrofísico Fco. Sánchez, E-38205 La Laguna, Tenerife, Spain

<sup>3</sup> INAF - Osservatorio di Astrofisica e Scienza dello Spazio di Bologna, Via Gobetti 93/3, I-40129 Bologna, Italy

<sup>4</sup> INAF – Osservatorio Astronomico di Roma, Via Frascati 33, 00078 Monte Porzio Catone, Roma, Italy

<sup>5</sup> INAF – Osservatorio Astronomico di Abruzzo, Via M. Maggini, 64100 Teramo, Italy

<sup>6</sup> INFN - Sezione di Pisa, Università di Pisa, Largo Pontecorvo 3, 56127 Pisa, Italy

<sup>7</sup> Instituto de Astrofísica de Canarias, Calle Vía Láctea s/n, E-38206 La Laguna, Tenerife, Spain

<sup>8</sup> Dipartimento di Fisica e Astronomia, Università degli Studi di Bologna, Via Piero Gobetti 93/2, 40129 Bologna, Italy

<sup>9</sup> Universidad de Granada, Departamento de Física Teórica y del Cosmos, Campus Fuente Nueva, Edificio Mecenas, 18071 Granada, Spain

<sup>10</sup> INAF - Osservatorio Astrofisico di Arcetri, Largo E. Fermi 5, I-50125 Firenze, Italy

<sup>11</sup> Astrophysics Research Institute, Liverpool John Moores University, 146 Brownlow Hill, Liverpool L3 5RF, UK

March 3, 2025

### ABSTRACT

We present the age determination of 13 globular clusters dynamically associated with the Gaia-Sausage-Enceladus (GSE) merger event, as part of the CARMA project effort to trace the Milky Way assembly history. We used deep and homogeneous archival *Hubble Space Telescope* data, and applied isochrone-fitting to derive homogeneous age estimates. We find that the majority of the selected clusters form a well-defined age-metallicity relation, with a few outliers. Among these, NGC 288 and NGC 6205 are more than 2 Gyr older than the other GSE globular clusters at similar metallicity, and are therefore interpreted as of likely in-situ origin. Moreover, NGC 7099 is somewhat younger than the average GSE trend, this suggesting a possible alternative dwarf galaxy progenitor, while NGC 5286 is mildly older, as if its progenitor was characterised by a higher star-formation efficiency. Another remarkable feature of the resulting age-metallicity relation is the presence of two epochs of globular cluster formation, with a duration of  $\sim 0.3$  Gyr each and separated by  $\sim 2$  Gyr. These findings are in excellent agreement with the age-metallicity relation of halo field stars found by González-Koda et al., clearly hinting at episodic star-formation in GSE. The age of the two formation epochs is similar to the mean age of the two groups of in-situ globular clusters previously studied by CARMA. These epochs might therefore be precisely pinpointing two important dynamical events that Gaia-Sausage-Enceladus had with the Milky Way during its evolutionary history. Finally, we discuss the correlation between the recent determination of Si and Eu with the clusters age and origin.

**Key words.** Galaxy: evolution – globular clusters: Gaia Enceladus – Galaxy: structure – techniques: photometric

### 1. Introduction

The quest for reconstructing the Milky Way (MW) assembly history is experiencing a revolution that started with the data release 2 of the *Gaia* mission (Gaia Collaboration et al. 2018). In fact, with the availability of 5D phase-space information, complemented by the line-of-sight velocities provided by large spectroscopic surveys such as APOGEE (Majewski et al. 2017), GALAH (De Silva et al. 2015), the Gaia ESO Survey (Gilmore et al. 2012), H3 (Conroy et al. 2019), and LAMOST (Cui et al. 2012), the possibility to study the orbital properties of nearby halo stars has led to the discovery and characterisation of past merger

events that have shaped the MW to its current appearance. It is now clear that the nearby halo is dominated by the remnant of the latest significant merger with the Gaia-Sausage-Enceladus (GSE) dwarf galaxy (Helmi et al. 2018; Belokurov et al. 2018). Additional contributions come from several less massive mergers like Sagittarius (Ibata et al. 1994), Sequoia (Myeong et al. 2019), the Helmi streams (Helmi et al. 1999), Antaeus (Oria et al. 2022; Ceccarelli et al. 2024a) and other candidates associated to coherent substructures in the integrals of motion space (see e.g. Massari et al. 2019; Koppelman et al. 2019; Horta et al. 2021; Malhan et al. 2022; Dodd et al. 2023; Mikkola et al. 2023).

However, it has become increasingly evident that the interpretation of sub-structures in the dynamical space is complicated by the fact that the debris of merger events naturally overlap (see e.g., Jean-Baptiste et al. 2017; Koppelman et al. 2020; Chen & Gnedin 2024; Mori et al. 2024), and that the same merger can create different coherent dynamical substructures, just like in-situ disc stars can do when perturbed by a massive merger (see e.g., Amarante et al. 2022; Khoperskov & Gerhard 2022; Belokurov et al. 2023). Ultimately, a purely dynamical selection produces samples of merger debris that are neither pure nor complete (Buder et al. 2022; Rey et al. 2023), and should be complemented by additional information on other conserved properties like chemistry (see e.g., Naidu et al. 2020; Horta et al. 2020; Ceccarelli et al. 2024a) or age (see e.g., Montalbán et al. 2021; Xiang & Rix 2022; Queiroz et al. 2023).

In this sense, globular clusters (GCs) play an important role, as they are the tracers of the MW assembly history for which age can be measured in the most precise way (see e.g., VandenBerg et al. 2013; Massari et al. 2023). With such a precise measurement, the age-metallicity relation (AMR) of MW GCs has proved to be a powerful tool to assess the origin of GCs as in-situ or accreted stellar systems (see e.g., Marín-Franch et al. 2009; Forbes & Bridges 2010; Leaman et al. 2013; Kruijssen et al. 2019; Massari et al. 2019; Callingham et al. 2022). Unfortunately, precise GC age measurements are limited to relatively small samples. Different age indicators, photometric systems, assumptions on distance, reddening and metallicity, and theoretical models are just some of the many sources of systematic uncertainties that affect different compilations of GC ages and that might pile up to  $\sim 2$  Gyr (Massari et al. 2019). To overcome these limitations, the CARMA project (Massari et al. 2023, hereafter Paper I) has started an effort to derive accurate ages for the entire system of MW GCs, based on isochrone fitting of each GC colour magnitude diagram (CMD) built by using homogeneous optical photometry taken with the *Hubble Space Telescope* (HST), and adopting the most up-to-date set of homogeneous theoretical models provided by the BaSTI database (Hidalgo et al. 2018; Pietrinferni et al. 2021).

In the first, proof-of-concept paper of the series, we have shown the power of our method applied to the pair of GCs NGC 6388 and NGC 6441, for which neither dynamics (Massari et al. 2019; Callingham et al. 2022) nor chemistry (Horta et al. 2020; Minelli et al. 2021; Carretta & Bragaglia 2022) could unambiguously determine the origin. By comparing their relative age with that of other four GCs with a clear in-situ origin, and with the AMR of halo field stars in the solar neighbourhood, we demonstrated that both GCs were born in-situ in the MW. In this second paper of the series, we focus on the GC population of the GSE merger (Helmi et al. 2018; Belokurov et al. 2018). GSE is the latest significant accretion event experienced by the MW about 9-11 Gyr ago (see e.g., Di Matteo et al. 2019; Gallart et al. 2019; Kruijssen et al. 2019; Naidu et al. 2021). Its stellar mass estimates range from a few  $\times 10^8 M_{\odot}$  (e.g., Lane et al. 2023) to some  $\times 10^9 M_{\odot}$  (e.g., Fattahi et al. 2019; Das et al. 2020). Its accretion seems to have had a dramatic impact on the evolution of the MW, as it led, for example, to the appearance of the thick disc as we currently know it (Helmi et al. 2018; Gallart et al. 2019; Ciucă et al. 2024). Due to its high mass, GSE likely hosted a large system of GCs, the current number of candidate members varying between 20

and 26 (Massari et al. 2019; Forbes 2020; Callingham et al. 2022; Chen & Gnedin 2024). Starting from a sub-sample of likely GSE members with publicly available HST photometry, we look for improving the uncertainty on the individual GC associations, and for assessing some of the properties of the GSE dwarf galaxy from the findings about the AMR of its GC system.

The paper is organised as follows. Section 2 summarizes the methods and the data used in this work. Section 3 presents the results of our GC age-dating and interprets the age-metallicity relation (AMR) of GSE GCs. Finally, a discussion on the most relevant findings is offered in Section 4. We remark that the results of the isochrone fit of each individual CMD are shown in the Appendix.

## 2. Data and methodology

The approach adopted in this work strictly follows the analysis presented in Paper I, extending it to a sample of *bona fide* GSE clusters. One of the most important keys of the CARMA project is homogeneity, both in the data (source, data reduction, calibration), theoretical models (complete and self consistent framework of the BaSTI library), and methods. We briefly summarize the specific aspects relevant for the current work.

### 2.1. Gaia-Enceladus globular cluster data

The sample includes 13 out of the 17 GCs associated to GSE according to both Massari et al. (2019) and Callingham et al. (2022). The four remaining clusters are ESO-SC06, NGC 6235 and NGC 6864 (excluded because no publicly available deep HST/ACS photometry exists) and NGC 5139 ( $\omega$  Cen, which will be analysed in a separate work due to the complexity of its stellar populations). The sample is listed in Table 1, which summarizes the name of the target and the derived values of metallicity, reddening, distance modulus and age.

The photometry used in this work comes from the public database of the HUGS project (Piotto et al. 2015). In particular, we used the *F606W* and *F814W* catalogues labelled as "method-2" (see also Anderson et al. 2008; Nardiello et al. 2018). The reasons for this choice are numerous and described in detail in Paper I, but in summary this photometric system is the only one common to almost all MW GCs, and these catalogues offer typically the deepest CMD. Additionally, this band combination is the least sensitive to the presence of multiple evolutionary sequences caused by chemically peculiar stellar populations. The original HUGS catalogues were processed in order to have the cleanest possible sample of stars in order to perform a reliable comparison with theoretical isochrones: *i*) only stars with membership probability larger than 90% were retained; *ii*) the apparent magnitudes were corrected for differential reddening using the method described in Milone et al. (2012); *iii*) sources in the innermost regions were removed to avoid poor photometric measurements due to crowding (20 to 60" depending on the cluster); *iv*) highly peculiar populations (such as those enriched significantly in C+N+O or He) were removed by identifying them in the multi-band chromosome maps (Milone et al. 2017).

## 2.2. Age estimates

The age derivation was performed by means of an isochrones fitting approach, following the procedures described in detail in Paper I. Briefly, we adopted theoretical models from the latest release of the BaSTI stellar evolution library (Hidalgo et al. 2018; Pietrinferni et al. 2021), covering a fine grid in age and metallicity. Age spans a wide range from 6 to 15 Gyr in steps of 100 Myr, and metallicity spans from -2.5 dex to 0.0 dex in steps of 0.01 dex. Solar-scaled models including diffusion were consistently used. We remark that the choice of solar-scaled models has been made to avoid making any assumptions on the  $\alpha$ -element abundance of GCs, which is an information either prone to large systematic errors due to very different literature sources, or entirely missing. We effectively absorb the term on the  $\alpha$ -element abundance by working in global metallicity  $[M/H]$ , rather than in iron abundance  $[Fe/H]$ . This is particularly justified by the fact that the photometry we analyse is in optical bands, for which the equivalency between solar-scaled and  $\alpha$ -enhanced models *at the same global metallicity* has been demonstrated by Salaris et al. (1993); Cassisi et al. (2004) through the relation:

$$[M/H] = [Fe/H] + \log(0.694 \times 10^{[\alpha/Fe]} + 0.301). \quad (1)$$

Finally, since some of the clusters are affected by large extinction, we applied a temperature-dependent reddening correction (see Girardi et al. 2008) to the models for clusters with  $E(B-V) > 0.1$  mag.

The values of the gaussian priors used by the code for the distance modulus (DM), metallicity and colour excess ( $E(B-V)$ ) are adopted from the Harris catalogue (Harris 2010). The dispersion associated to each parameter is assumed as follows:  $\sigma_{DM} = 0.1$  mag,  $\sigma_{[M/H]} = 0.1$  dex,  $\sigma_{E(B-V)} = 0.05$  mag. The adoption of the same dispersion for all GCs is justified by the fact that these values are conservative numbers, and are typically associated as uncertainties to the Harris compilation over the entire MW GC sample, whereas the GCs analysed here are typically nearby, poorly extinct, and with existing, high-precision photometric and spectroscopic investigations. For each individual GC, two separate isochrone fitting solutions are obtained for the  $(m_{F606W}, m_{F606W}-m_{F814W})$  and  $(m_{F814W}, m_{F606W}-m_{F814W})$  CMDs. As the final result, we use the average value of the two solutions (which are shown for each individual GC in the Appendix), while the overall uncertainties are computed such to encompass the upper and lower limits of both runs combined. We finally remark that the age values presented here should be interpreted strictly in a relative sense.

## 3. Results

Figure 1 presents the results of the isochrone fit for NGC 288 as an example. Similar plots for the other clusters are presented in the Appendix. The plot displays the solution derived in both CMDs:  $(m_{F814W}, m_{F606W}-m_{F814W})$  and  $(m_{F606W}, m_{F606W}-m_{F814W})$  in the left and right columns, respectively. The top panels present the best fitting isochrone superposed to each CMDs, while the bottom panels show the posterior distributions of the parameters of the model, including their correlation. The corner plots report the best fit values for the metallicity, reddening, distance modulus and age.

In addition to the quality selection described in Sect. 2.1, for each CMD the stars effectively fit have been selected within a colour range from the mean-ridge line, thus to exclude obvious binaries, blue straggler stars and residual outliers. Gray and green points in the CMD show, respectively, the sources retained after the quality cuts, and those used in the fit. The lower and upper magnitude cuts were optimized on a cluster-by-cluster basis, to reach a balance between the number of red giant branch (RGB, driving the solution in  $[M/H]$ ) and main sequence (MS, most sensitive to age) stars. In fact, we found that for the most massive GCs, a brighter cut in MS helped the code in reaching a solution in  $[M/H]$  more consistent with spectroscopic values available in the literature. The plots for NGC 288 (and similarly for all the other targets) display a good isochrone fit from the tip of the RGB down to the faint MS stars. The corner plot shows typically a well defined minimum for the four output parameters.

The results of the isochrone fitting in terms of  $[M/H]$ ,  $E(B-V)$ ,  $(m-M)_0$ , and age for the 13 GCs under analysis are summarised in Table 1. Figure 2 shows the difference between literature values from the Harris catalogue<sup>1</sup> and the outcome of the isochrone fitting for distance, reddening, and metallicity for the 13 clusters. Note that the global metallicity  $[M/H]$  that we find as output of the fit has been translated to iron abundance  $[Fe/H]$  according to Equation 1 and by using the  $[\alpha/Fe]$  vs.  $[Fe/H]$  trend observed in GSE stars (see Helmi et al. 2018), well described by the relation  $[\alpha/Fe] = -0.2 \times [Fe/H]$  for  $-2.5 < [Fe/H] < -0.5$ . The solid and dashed lines represent the mean difference and the  $1-\sigma$  dispersion. For all three parameters, the mean difference is always consistent with zero within  $1-\sigma$ . This is also true when referring the comparison to the distance modulus values found in (Baumgardt & Vasiliev 2021), in which case we find a mean difference of  $\Delta = -0.01$  with  $\sigma = 0.03$ . In general, no particularly pathologic cases are evident, this supporting the validity of the solutions found. Moreover, the dispersion around the mean of the three distributions matches the typical uncertainties associated to each data point. This is an indication that these uncertainties, computed as the sum in quadrature between those provided in Table 1 and those from the Harris (1996) catalogue (see also Paper I), are a fair representation of the actual ones.

### 3.1. The GSE age-metallicity relation

Fig. 3 shows the age-metallicity relation for our sample of GSE GCs. For reference, the location of the in-situ GC analysed by (Paper I) is also indicated with gray symbols. This AMR clearly shows some remarkable features:

*i)* the youngest GSE GCs are significantly more metal-poor compared to the in-situ GCs of similar age. This is an expected property, as dwarf galaxies like GSE form stars with a lower efficiency compared to the MW, and lose a larger fraction of metals due to the shallower gravitational potential. As a result of these effects combined, the chemical evolution of GSE reaches a lower metallicity compared to the MW in the same amount of time (this manifesting in the mass-metallicity relation, see e.g. Kirby et al. 2013; Kruijssen et al. 2019).

<sup>1</sup> we refer to the 2010 edition, which provides GC properties with reasonable homogeneity, at least for the sample of GCs analysed here.

Table 1: Results of the isochrone fitting.

Name	[M/H]	E(B-V) [mag]	DM [mag]	age [Gyr]
NGC 288	-1.12 $^{+0.08}_{-0.08}$	0.02 $^{+0.01}_{-0.01}$	14.77 $^{+0.01}_{-0.01}$	13.75 $^{+0.28}_{-0.22}$
NGC 362	-1.16 $^{+0.03}_{-0.04}$	0.03 $^{+0.01}_{-0.01}$	14.79 $^{+0.01}_{-0.01}$	11.47 $^{+0.11}_{-0.10}$
NGC 1261	-1.20 $^{+0.05}_{-0.02}$	0.01 $^{+0.01}_{-0.01}$	16.06 $^{+0.01}_{-0.01}$	11.81 $^{+0.06}_{-0.13}$
NGC 1851	-1.05 $^{+0.01}_{-0.01}$	0.04 $^{+0.01}_{-0.01}$	15.39 $^{+0.02}_{-0.01}$	11.41 $^{+0.05}_{-0.06}$
NGC 2298	-1.64 $^{+0.11}_{-0.03}$	0.22 $^{+0.01}_{-0.01}$	14.93 $^{+0.02}_{-0.02}$	13.09 $^{+0.41}_{-0.35}$
NGC 2808	-1.04 $^{+0.01}_{-0.01}$	0.22 $^{+0.01}_{-0.01}$	15.01 $^{+0.01}_{-0.01}$	11.09 $^{+0.11}_{-0.10}$
NGC 5286	-1.47 $^{+0.04}_{-0.04}$	0.25 $^{+0.01}_{-0.01}$	15.20 $^{+0.01}_{-0.01}$	13.47 $^{+0.17}_{-0.05}$
NGC 5897	-1.58 $^{+0.09}_{-0.08}$	0.12 $^{+0.01}_{-0.00}$	15.52 $^{+0.02}_{-0.02}$	13.10 $^{+0.22}_{-0.46}$
NGC 6205	-1.29 $^{+0.07}_{-0.08}$	0.01 $^{+0.01}_{-0.01}$	14.34 $^{+0.03}_{-0.03}$	14.06 $^{+0.35}_{-0.41}$
NGC 6341	-1.77 $^{+0.08}_{-0.09}$	0.01 $^{+0.01}_{-0.01}$	14.59 $^{+0.02}_{-0.02}$	13.58 $^{+0.22}_{-0.21}$
NGC 6779	-1.67 $^{+0.04}_{-0.02}$	0.24 $^{+0.01}_{-0.01}$	15.07 $^{+0.01}_{-0.01}$	13.52 $^{+0.22}_{-0.20}$
NGC 7089	-1.41 $^{+0.02}_{-0.02}$	0.05 $^{+0.01}_{-0.01}$	15.32 $^{+0.01}_{-0.01}$	12.75 $^{+0.29}_{-0.09}$
NGC 7099	-1.83 $^{+0.02}_{-0.02}$	0.04 $^{+0.01}_{-0.01}$	14.61 $^{+0.01}_{-0.01}$	13.05 $^{+0.12}_{-0.09}$

**Notes.** The CMD fits and the corner plots are shown in Figure 1 and in the Appendix.

*ii)* most of the GSE GCs describe a very tight AMR, that covers a total lifespan of 2.5 Gyr, with a handful of possible outliers;

*iii)* the most obvious outliers are NGC 288 and NGC 6205 (M 13), which we find to be more than 2 Gyr older compared to the other GSE GCs at the same metallicity. The old age of NGC 288 is not a novel finding, but has been debated since the nineties. Both Green & Norris (1990) and Sarajedini & Demarque (1990) found it to be older than NGC 362 by 2-3 Gyr. This finding was later challenged by Stetson et al. (1996), who found no age difference between the two GCs. Later investigations (including e.g., Bellazzini et al. 2001; Marín-Franch et al. 2009; VandenBerg et al. 2013) resulted in a range of age values, which we settle in this work. An age difference of  $> 2.5$  Gyr compared to the four younger GSE GCs (which include NGC 362) clearly advocates for a different origin for NGC 288, likely an in-situ one. A more detailed and conclusive analysis of this hypothesis, based on additional high-resolution spectroscopic data, is presented in a forthcoming paper (Ceccarelli et al. in prep.). Also in the case of NGC 6205, previous homogeneous relative age determinations resulted in conflicting conclusions. VandenBerg et al. (2013) found it to be about as old as NGC 288 and more than 1 Gyr older than

other GSE GCs at similar metallicity like NGC 1261 and NGC 362, which is qualitatively consistent with our findings. On the other hand, Marín-Franch et al. (2009) classified it among the young GCs, even if for these authors, too, NGC 6205 is  $\sim 10\%$  older than NGC 1261 and NGC 362. Interestingly, the classifications of Belokurov & Kravtsov (2024) and Chen & Gnedin (2024) (that use [Al/Fe] as a criterion) provide opposite results for the in-situ or accreted origin of NGC 6205, whereas our findings indicate a likely in-situ origin. For these reasons, hereafter we exclude both NGC 288 and NGC 6205 from the analysis of purely GSE GCs;

*iv)* The other possible outliers are NGC 5286, which is somewhat older compared to the trend defined by the majority of the GSE sample, and NGC 7099, which is instead slightly younger. One possibility is that these two GCs are in fact genuine members of the GSE population, in which case their location in the AMR might be indicative of a somewhat inhomogeneous metallicity distribution, or of a metallicity gradient, in the primordial GSE dwarf. Alternatively, these two GCs might be contaminating the sample of pure GSE GCs. In case the two GCs are contaminants, NGC 7099 should belong to a merger event that formed with a lower star-formation efficiency compared to GSE

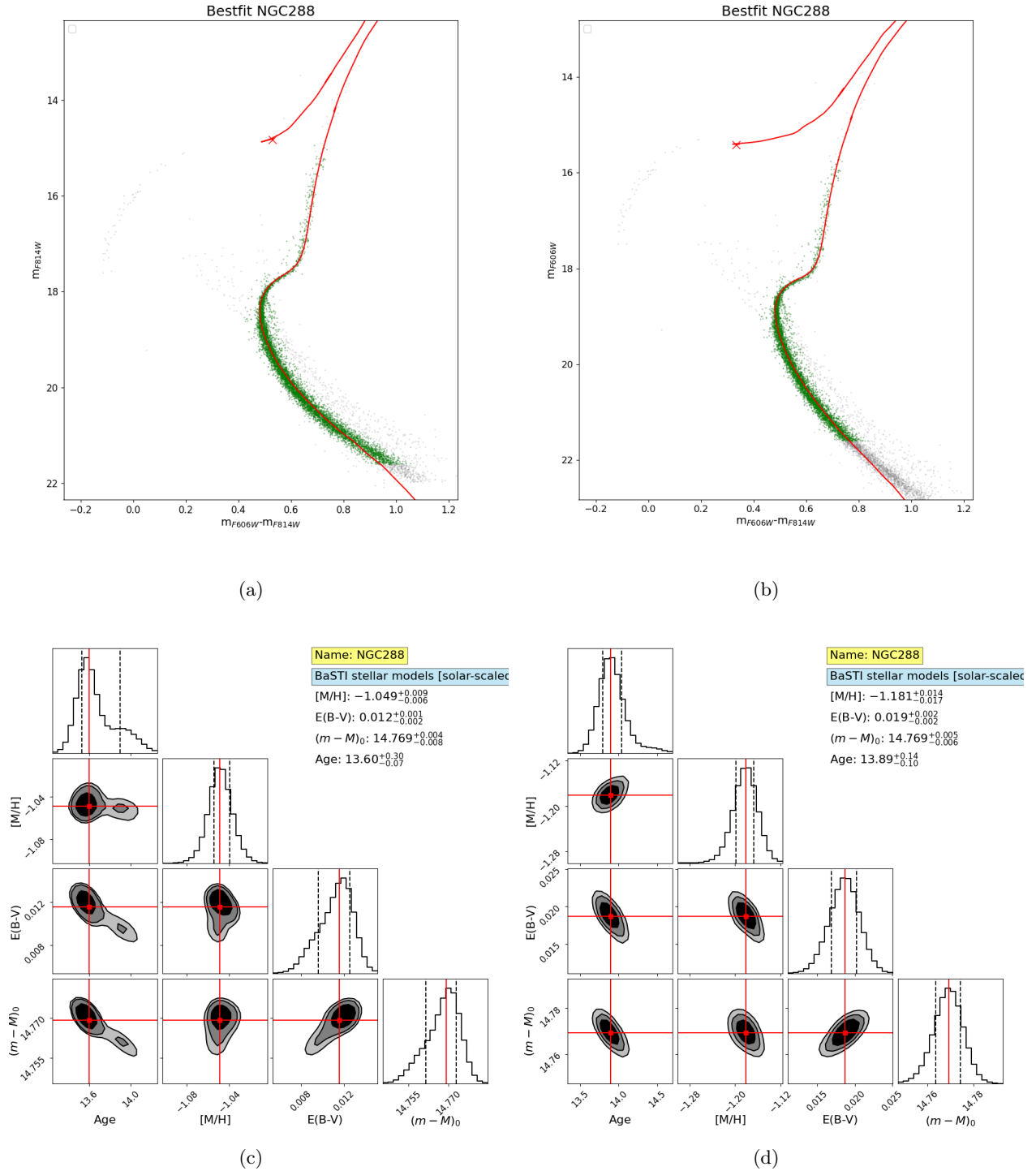


Fig. 1: Results for NGC 288. Panel (a): Best fit model in the  $(m_{F814W}, m_{F606W}-m_{F814W})$  CMD. Panel (b): Best fit model in the  $(m_{F606W}, m_{F606W}-m_{F814W})$  CMD. Panel (c): Posterior distributions for the output parameters and the best-fit solution, quoted in the labels, in the  $(m_{F814W}, m_{F606W}-m_{F814W})$  CMD. Panel (d): Posterior distributions for the output parameters and the best-fit solution, quoted in the labels, in the  $(m_{F606W}, m_{F606W}-m_{F814W})$  CMD.

(see the AMR models in e.g., Massari et al. 2019; Callingham et al. 2022; Souza et al. 2024), like Sequoia or the Helmi streams. Given its retrograde orbit<sup>2</sup> at  $E = -173969$

$\text{km}^2/\text{s}^2$  and  $L_z = -252 \text{ km/s kpc}$ , Sequoia seems the most likely candidate. On the other hand, NGC 5286 should belong to a galaxy that formed stars more efficiently than

<sup>2</sup> these values are computed based on the proper motion values in Vasiliev & Baumgardt (2021) and distances in Baumgardt

& Vasiliev (2021), and following the same prescriptions as in Massari et al. (2019).

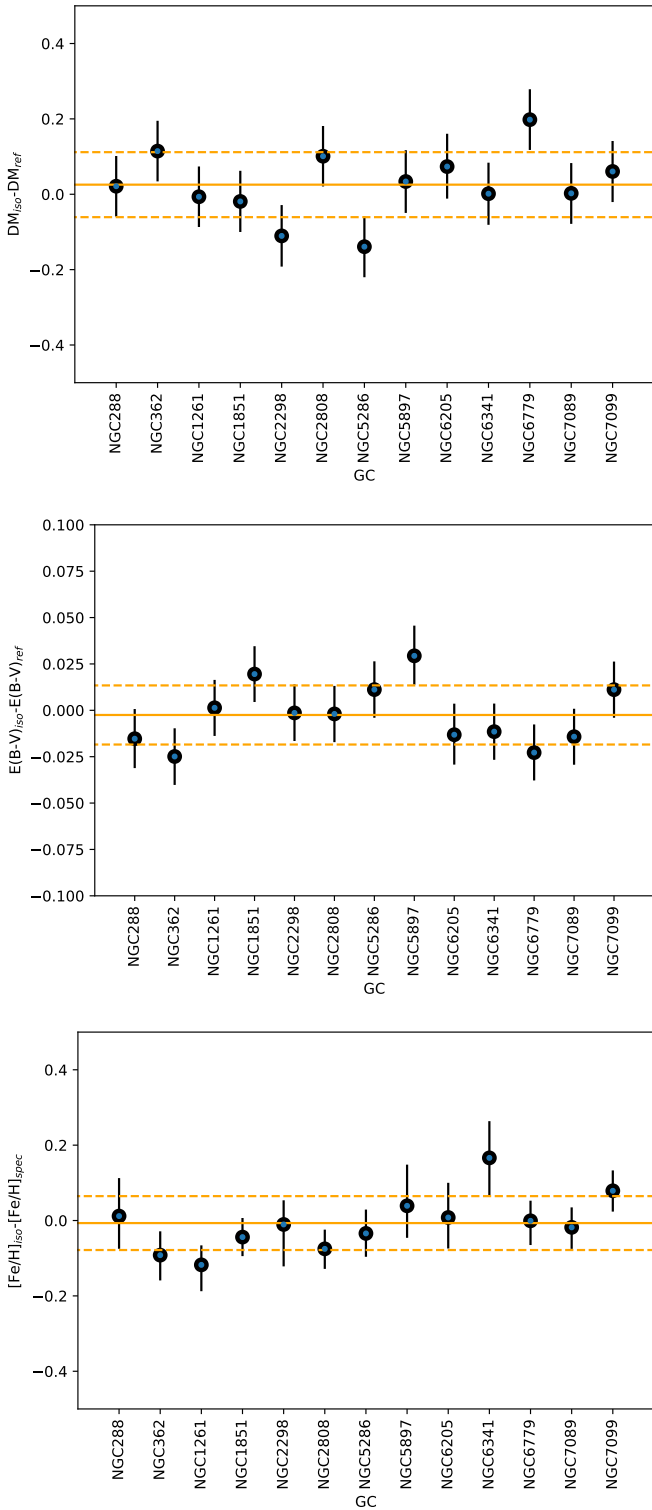


Fig. 2: Difference between literature values and the parameters obtained as output of the isochrone fitting for the true distance modulus (top panel), colour excess (middle panel), and metallicity (bottom panel). The solid and dashed lines mark the mean value and the dispersion around the mean of each distribution.

GSE, and the only possibilities are either Kraken (Massari et al. 2019; Kruijssen et al. 2020) or the MW itself. Chem-

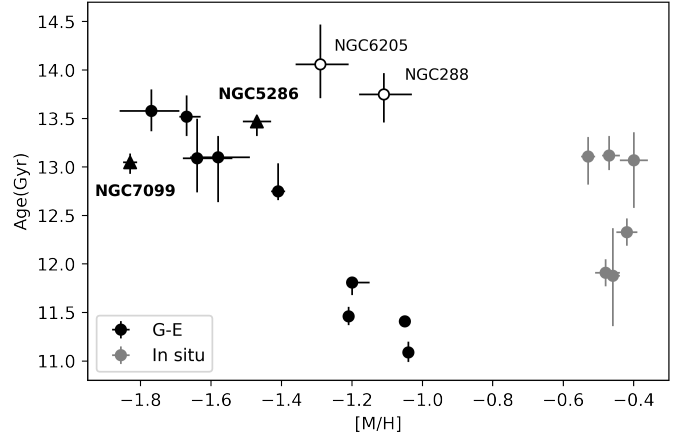


Fig. 3: AMR of our sample of dynamically selected GSE GCs. Candidate in-situ clusters (namely NGC 288 and NGC 6205) are shown as open circles. GCs with uncertain membership to GSE (namely NGC 5286 and NGC 7099) are shown as black filled triangles. The metal-rich, in-situ GCs analysed in Paper I are shown in gray for the sake of comparison.

istry does not provide yet a conclusive way of resolving these doubts (e.g., Monty et al. 2024), as no homogeneous derivation of elemental abundances sensitive to the GC origin at this intermediate metallicity (like Mg, Ca, Ti, Zn, Eu, see Ceccarelli et al. 2024b) exist. Future addition by the CARMA project of the age of GCs from different progenitors will shed light on the actual origin of NGC 7099 and NGC 5286;

*v)* finally, the AMR of the remaining nine genuine members of GSE clearly shows evidence for two events of GC formation, separated by about 2 Gyr. The earlier one happened at  $t \simeq 13.2$  Gyr ( $\sigma=0.3$  Gyr), and is responsible for the formation of NGC 2298, NGC 5897, NGC 6341, NGC 6779, and NGC 7089. The later one took place at  $t \simeq 11.4$  Gyr ( $\sigma=0.3$  Gyr), and originated NGC 362, NGC 1261, NGC 1851 and NGC 2808. It is interesting to note that these young GSE GCs formed at about the same time as the young in-situ GCs, that formed at  $t \simeq 12$  Gyr. This might be evidence for these almost simultaneous events of GC formation to have been caused by the same trigger. We discuss these features further in light of a comparison with the AMR of GSE stars in the next Section 3.2.

### 3.2. Comparison with field stars

González-Koda et al. (2024, *subm.*, hereafter GK2024) have analyzed the age-metallicity distribution of GSE field stars within a volume of 1.2 kpc from the Sun. They dynamically selected three samples of GSE stars within this volume with different criteria and possible levels of contamination, either in action-angle coordinates (following Feuillet et al. 2021; Horta et al. 2024), or using a single-linkage clustering algorithm as in Dodd et al. (2023). In Fig. 4 we show the superposition of the eleven likely GSE GCs ages and metallicities and the stellar age-metallicity distribution derived for the field stars of the sample named "GSE-group" in GK2024, which is the intermediate of their three samples in terms of number of stars and possible degree of contamination.

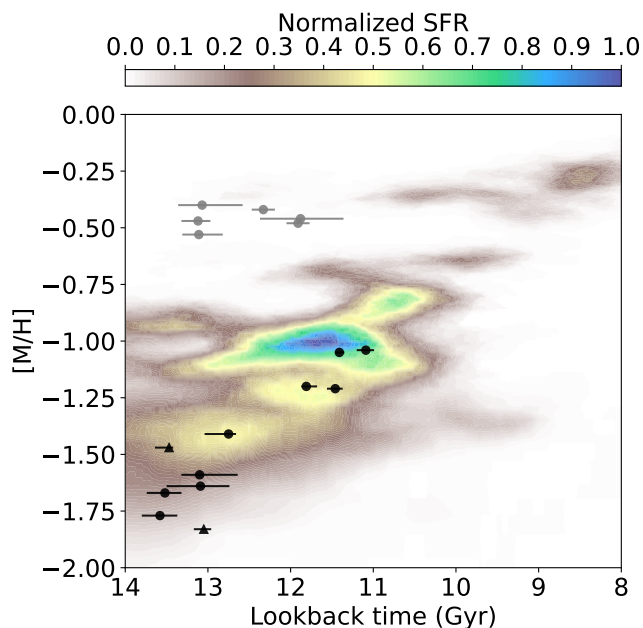


Fig. 4: Comparison between the AMRs of the most likely GSE GCs (black symbols) and stars (density map, González-Koda et al.). The location of the six in-situ GCs studied in Paper I is also shown with gray symbols as reference.

The two AMRs are remarkably similar in terms of their slope, and there is evidence for similarly bursty distributions (even though GK2024 warn about the fact that the bursty behaviour of the age-metallicity distribution has to be taken with caution due to the low number statistics which can affect the solution). However, providing a direct comparison between the location of the star-formation peaks is tricky, because both the methods and the data used to determine the two AMRs are entirely different. The size of the possible systematic offsets in age and metallicity due to these differences have been estimated in GK2024 under different assumptions (see their Appendix C for details). Briefly, the possible offsets are quantified applying their CMD fitting technique (CMDft.Gaia) to GSE GCs stars using purely *Gaia* data and a similar approach to that followed for the analysis of GSE field stars. However, we remark that it is basically impossible to perfectly replicate the CMD fitting technique on GCs photometry, as for example the distance of the relatively nearby field stars used in that work can be determined robustly from *Gaia* parallaxes, while both crowding issues and the larger distance of the GCs make the same *Gaia* parallaxes very inaccurate for GC stars (see e.g., Pancino et al. 2017). Additionally, the reddening of the field stars is determined from 3D reddening maps (Lallement et al. 2018; Green et al. 2019) which do not reach the distance of the clusters and thus all-sky 2D maps are used to estimate their reddening, which may be thus non-homogeneous with that of field stars. Therefore, such an investigation should be considered as evidence that systematic differences might be at play, but that they are difficult to quantify precisely. In spite of these possible offsets (found to be of a maximum of  $\simeq 1$  Gyr in age and  $\simeq$

0.2 dex in metallicity) the agreement between the ages and metallicities of the clusters and those of the main features in the AMR of field stars is remarkable. There is marginal evidence that the old peak of GC formation might be related to the most metal-poor signal in the stellar AMR, located at  $t \gtrsim 12.5$  and  $[M/H] \lesssim -1.4$ , whereas the young peak of GC formation could be related to the most evident episode of star formation at  $t \sim 11.8$  and  $[M/H] \sim -1.0$ . The combination of these complementary but totally independent studies provides further evidence for the existence of episodic star formation in GSE. This kind of events are predicted to be related to the dynamical interactions between the incoming merging galaxy and the host (Di Cintio et al. 2021; Orkney et al. 2022). The exact correlation between a burst in star-formation and a dynamical event like the pericentric passage, a fly-by or the final coalesce phase is not straightforward, though (see, e.g., Di Matteo et al. 2008). It might depend on the orbital properties of the merger, as well as on its gas content and mass (Di Cintio et al. 2021). Simulations of dwarf galaxy mergers (e.g., Walker et al. 1996; Di Matteo et al. 2008; Villalobos & Helmi 2008) show that the typical separation between the first and second pericentric passages is of 0.5-1 Gyr, whereas the separation between the first pericentric passage and the final coalescence of the dwarf galaxy into the host can reach up to  $\sim 2$  Gyr.

We are thus inclined to interpret the two observed peaks in the GC age distribution in terms of two possibilities:

- i*) The first peak of GC formation happened when GSE was experiencing its very early evolution in isolation, while the second peak coincide with one particular dynamical event of interaction with the MW, being this either the first pericentric passage, or the phase of final coalescence. This interpretation finds support in the results by GK2024, where the population called GSE0 by the authors shares a similar location in the AMR with the most metal-poor GCs of the first peak;
- ii*) Both peaks are originated by the dynamical interaction with the MW, and given the separation of 2 Gyr, we favour the scenario according to which the first burst coincides with the first pericentric passage and the second one with the coalescence phase.

In both cases, it is interesting to note that the duration of the two burst we found is of  $\sim 300$  Myr, which is the average duration for star-forming bursts found by Di Matteo et al. (2008) in their suite of simulations. Moreover, the age of the two peaks of GSE GCs formation is rather similar to the mean age of the two groups of in-situ GCs discussed in Paper I and shown in Fig. 3. This could be indicative that GC formation in both the host (the MW) and the accreting dwarf (GSE) might have been triggered by the mutual dynamical interaction, in agreement with predictions for stars from simulations (Di Cintio et al. 2021). If this purely tentative interpretation were confirmed, our age estimates would provide a very precise and dynamically-independent measurement of the timescale related to the dynamical evolution of the GSE merger.

### 3.3. The $[Eu/Si]$ trend of GSE GCs

The AMR described by our sample of GCs has allowed us to select nine GCs genuinely associated with GSE (namely NGC 362, NGC 1261, NGC 1851, NGC 2298, NGC 2808, NGC 5897, NGC 6341, NGC 6779 and NGC 7089) and two additional ones (NGC 7099 and NGC 5286) whose associ-

ation is more uncertain, but that very likely belong to the accreted MW GC population given their age and dynamical properties. Monty et al. (2024) used the  $[\text{Eu}/\text{Si}]$  abundance ratio as a chemical tool to distinguish between accreted and in-situ MW GCs. Moreover by linking the  $[\text{Eu}/\text{Si}]$  trend for the sample of GSE GCs defined in Myeong et al. (2019) with the age estimates by VandenBerg et al. (2013), they found an observational way to time at high, sub-Gyr resolution the star-formation history of the GSE dwarf galaxy. We are now in a position to leverage on our findings to improve even further upon these results, by investigating a very pure sample of GSE GCs (14 out of the 21 GSE GC members according to Myeong et al. 2019 do not belong to our set of 9 genuine members) and using extremely high-precision relative age. The results about the  $[\text{Eu}/\text{Fe}]$ ,  $[\text{Si}/\text{Fe}]$  and  $[\text{Eu}/\text{Si}]$  trends as a function of age are shown in Fig. 5, where the abundances are the same as those used by Monty et al. (2024).

The first interesting feature is that NGC 5286, that as described in Sect. 3.1 could be a contaminant of the GSE GC sample belonging to a galaxy that formed stars with higher star-formation efficiency, is the GC showing the lowest value of  $[\text{Eu}/\text{Si}]$  (see the top panel of Fig. 5). As described by the chemical evolutionary models in Monty et al. (2024), a low value of  $[\text{Eu}/\text{Si}]$  is exactly what should be expected for such a case. This evidence therefore support the idea that NGC 5286 might not be part of the GSE GC system. On the other hand, NGC 7099 (the other candidate contaminant) has a  $[\text{Eu}/\text{Si}]$  value consistent with that of the genuine GSE GCs at similar age. Not much can be drawn on its actual origin from this chemical space.

The second clear feature is that all the three chemical spaces show very tight abundance trends with age when considering genuine GSE GCs. In particular, in good agreement with Monty et al. (2024), our  $[\text{Eu}/\text{Si}]$  describes an increasing trend, that range from  $[\text{Eu}/\text{Si}] \sim -0.2$  at  $t=13.6$  Gyr, to  $[\text{Eu}/\text{Si}] \sim 0.4$  at  $t=11.1$  Gyr. A linear fit to the distribution of values leads to an increase rate of  $\delta[\text{Eu}/\text{Fe}] = 0.26 \text{ yr}^{-1}$ . The other two additional panels are best fit by rates of  $\delta[\text{Eu}/\text{Fe}] = -0.15 \text{ yr}^{-1}$  (see the dashed black line in the middle panel of Fig. 5), and  $\delta[\text{Si}/\text{Fe}] = -0.11 \text{ yr}^{-1}$  (see the dashed black line in the bottom panel), which can be useful constraints for chemical evolution models.

#### 4. Summary and Conclusions

In this second paper of the CARMA series, we have further demonstrated the power of precise age measurements in unravelling the complex history of the Milky Way's assembly through its system of GCs. Expanding on the methods and findings presented in Paper I, we applied the refined isochrone fitting technique to a sample of thirteen GCs dynamically associated to the GSE merger event (Massari et al. 2019; Callingham et al. 2022), aiming to accurately determine their ages and, by extension, to confirm their origin and to reconstruct some of the properties of the progenitor galaxy.

Our results show that the AMR of the GCs analysed in this study span a 3 Gyr-wide range of ages across  $\sim 1$  dex in metallicity. The unprecedented precision in the age determination allows us to clearly identify a few GCs that, despite their dynamical properties, are likely not members of the GSE GC system. The most obvious ones are NGC 288 and NGC 6205, that we find to be significantly older (by

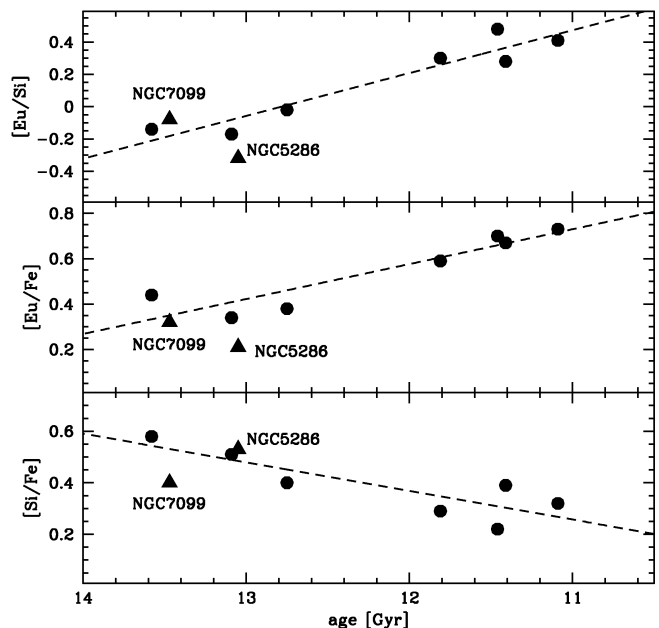


Fig. 5: Observed trends of  $[\text{Si}/\text{Fe}]$  (bottom panel),  $[\text{Eu}/\text{Fe}]$  (middle panel) and  $[\text{Eu}/\text{Si}]$  (top panel) as a function of age for our sample of accreted GC. The black triangles indicate the two GCs for which the association to GSE is uncertain given their age (see the corresponding labels). Chemical abundances are taken from the compilation in Monty et al. (2024).

2 Gyr or more) than the other GSE GCs at similar metallicity. This is a clear indication (e.g., Leaman et al. 2013; Kruijssen et al. 2019) that these two systems might have been born in the Milky Way, rather than in an accreted dwarf galaxy. Moreover, out of the remaining eleven likely accreted GCs, nine describe a very tight AMR, whereas two, namely NGC 7099 and NGC 5286, appear as outliers. While the location in the AMR plane, the retrograde orbit, and the  $[\text{Eu}/\text{Si}]$  abundance (Monty et al. 2024) of NGC 7099 still indicate a likely accreted origin, possibly from the Sequoia dwarf galaxy, the properties of NGC 5286 leave its association quite uncertain, with its possible progenitors being GSE itself, Kraken or the MW. In this respect, Belokurov & Kravtsov (2024) find the  $[\text{Al}/\text{Fe}]$  content of NGC 5286 to be consistent with an in-situ origin.

The remaining nine genuine members of GSE describe a well defined AMR that shows a remarkably clear bimodal distribution. The two peaks of GC formation are separated by  $\sim 2$  Gyr, have a duration (computed as the  $1\sigma$  age dispersion) of 0.3 Gyr, and their mean age is similar to that of the two groups of in-situ GCs studied in Paper I. The same slope and possible bursty features have been detected in the AMR of GSE field stars by González-Koda et al. in prep., using CMD fitting. Our interpretation is that these two bursts of star formation might be linked to the orbital properties of GSE, with the first pericentric passage and/or its final phase of coalescence with the MW being primary candidates as responsible for the star-formation triggers (Di Matteo et al. 2008). The earliest epoch of GC formation, whose location in the AMR matches remarkably well that



of GSE stars (Horta et al. 2024) as measured by Xiang & Rix (2022), might even correspond to the initial phase during which GSE evolved in isolation. In any case, our age estimates would provide a robust and independent measurement of the dynamical timescales of the GSE merger event. Finally, these nine GSE GCs describe tight trends in the chemical evolution of elements like Eu and Si, that we quantify in an attempt of providing tight constraints in chemical evolution models.

Our findings highlight the critical role of high-precision, homogeneous photometry, theoretical models and methods in enhancing the precision of GC relative age estimates, that are crucial in resolving ambiguities on the MW GCs origin, and therefore in depicting a detailed picture of our Galaxy assembly.

## Acknowledgements

DM, SC, and EP acknowledge financial support from PRIN-MIUR-22: CHRONOS: adjusting the clock(s) to unveil the CHRONO-chemo-dynamical Structure of the Galaxy” (PI: S. Cassisi). SS acknowledges funding from the European Union under the grant ERC-2022-AdG, "StarDance: the non-canonical evolution of stars in clusters", Grant Agreement 101093572, PI: E. Pancino. CG, TRL and SC acknowledge support from the Agencia Estatal de Investigación del Ministerio de Ciencia e Innovación (AEI-MCINN) under grant "At the forefront of Galactic Archaeology: evolution of the luminous and dark matter components of the Milky Way and Local Group dwarf galaxies in the Gaia era" with reference PID2020-118778GB-I00/10.13039/501100011033 and PID2023-150319NB-C21/C22/10.13039/501100011033. CG also acknowledge support from the Severo Ochoa program through CEX2019-000920-S. TRL acknowledges support from Juan de la Cierva fellowship (IJC2020-043742-I) and Ramón y Cajal fellowship (RYC2023-043063-I, financed by MCIU/AEI/10.13039/501100011033 and by the FSE+). M.M. acknowledges support from the Agencia Estatal de Investigación del Ministerio de Ciencia e Innovación (MCIN/AEI) under the grant "RR Lyrae stars, a lighthouse to distant galaxies and early galaxy evolution" and the European Regional Development Fun (ERDF) with reference PID2021-127042OB-I00. Co-funded by the European Union (ERC-2022-AdG, "StarDance: the non-canonical evolution of stars in clusters", Grant Agreement 101093572, PI: E. Pancino). Views and opinions expressed are however those of the author(s) only and do not necessarily reflect those of the European Union or the European Research Council. Neither the European Union nor the granting authority can be held responsible for them

Based on observations with the NASA/ESA HST, obtained at the Space Telescope Science Institute, which is operated by AURA, Inc., under NASA contract NAS 5-26555. This research made use of emcee (Foreman-Mackey et al. 2013). This work has made use of data from the European Space Agency (ESA) mission *Gaia* (<https://www.cosmos.esa.int/gaia>), processed by the *Gaia* Data Processing and Analysis Consortium (DPAC, <https://www.cosmos.esa.int/web/gaia/dpac/consortium>). Funding for the DPAC has been provided by national institutions, in particular the institutions participating in the *Gaia* Multi-lateral Agreement. This project has received funding from

the European Research Council (ERC) under the European Union’s Horizon 2020 research and innovation programme (grant agreement No. 804240) for S.S. and Á.S. M.M. acknowledges support from the Agencia Estatal de Investigación del Ministerio de Ciencia e Innovación (MCIN/AEI) under the grant "RR Lyrae stars, a lighthouse to distant galaxies and early galaxy evolution" and the European Regional Development Fun (ERDF) with reference PID2021-127042OB-I00, and from the Spanish Ministry of Science and Innovation (MICINN) through the Spanish State Research Agency, under Severo Ochoa Programme 2020-2023 (CEX2019-000920-S).

## References

- Amarante, J. A. S., Debattista, V. P., Beraldo e Silva, L., Laporte, C. F. P., & Deg, N. 2022, *ApJ*, 937, 12
- Anderson, J., Sarajedini, A., Bedin, L. R., et al. 2008, *AJ*, 135, 2055
- Baumgardt, H. & Vasiliev, E. 2021, *MNRAS*, 505, 5957
- Bellazzini, M., Pecci, F. F., Ferraro, F. R., et al. 2001, *AJ*, 122, 2569
- Belokurov, V., Erkal, D., Evans, N. W., Koposov, S. E., & Deason, A. J. 2018, *MNRAS*, 478, 611
- Belokurov, V. & Kravtsov, A. 2024, *MNRAS*, 528, 3198
- Belokurov, V., Vasiliev, E., Deason, A. J., et al. 2023, *MNRAS*, 518, 6200
- Buder, S., Lind, K., Ness, M. K., et al. 2022, *MNRAS*, 510, 2407
- Callingham, T. M., Cautun, M., Deason, A. J., et al. 2022, *MNRAS*, 513, 4107
- Carretta, E. & Bragaglia, A. 2022, *A&A*, 660, L1
- Cassisi, S., Salaris, M., Castelli, F., & Pietrinferni, A. 2004, *ApJ*, 616, 498
- Ceccarelli, E., Massari, D., Mucciarelli, A., et al. 2024a, *A&A*, 684, A37
- Ceccarelli, E., Mucciarelli, A., Massari, D., Bellazzini, M., & Matsuno, T. 2024b, arXiv e-prints, arXiv:2410.06702
- Chen, Y. & Gnedin, O. Y. 2024, *The Open Journal of Astrophysics*, 7, 23
- Ciucă, I., Kawata, D., Ting, Y.-S., et al. 2024, *MNRAS*, 528, L122
- Conroy, C., Bonaca, A., Cargile, P., et al. 2019, *ApJ*, 883, 107
- Cui, X.-Q., Zhao, Y.-H., Chu, Y.-Q., et al. 2012, *Research in Astronomy and Astrophysics*, 12, 1197
- Das, P., Hawkins, K., & Jofré, P. 2020, *MNRAS*, 493, 5195
- De Silva, G. M., Freeman, K. C., Bland-Hawthorn, J., et al. 2015, *MNRAS*, 449, 2604
- Di Cintio, A., Mostoghiu, R., Knebe, A., & Navarro, J. F. 2021, 506, 531
- Di Matteo, P., Bournaud, F., Martig, M., et al. 2008, *A&A*, 492, 31
- Di Matteo, P., Haywood, M., Lehnert, M. D., et al. 2019, *A&A*, 632, A4
- Dodd, E., Callingham, T. M., Helmi, A., et al. 2023, *A&A*, 670, L2
- Fattahi, A., Belokurov, V., Deason, A. J., et al. 2019, *MNRAS*, 484, 4471
- Feuillet, D. K., Sahlholdt, C. L., Feltzing, S., & Casagrande, L. 2021, *MNRAS*, 508, 1489
- Forbes, D. A. 2020, *MNRAS*, 493, 847
- Forbes, D. A. & Bridges, T. 2010, *MNRAS*, 404, 1203
- Foreman-Mackey, D., Hogg, D., Lang, D., & Goodman, J. 2013, *Publications of the Astronomical Society of the Pacific*, 125, 306
- Gaia Collaboration, Brown, A. G. A., Vallenari, A., et al. 2018, *A&A*, 616, A1
- Gallart, C., Bernard, E. J., Brook, C. B., et al. 2019, *Nature Astronomy*, 3, 932
- Gilmore, G., Randich, S., Asplund, M., et al. 2012, *The Messenger*, 147, 25
- Girardi, L., Dalcanton, J., Williams, B., et al. 2008, *PASP*, 120, 583
- Green, E. M. & Norris, J. E. 1990, *ApJ*, 353, L17
- Green, G. M., Schlafly, E., Zucker, C., Speagle, J. S., & Finkbeiner, D. 2019, *ApJ*, 887, 93
- Harris, W. E. 1996, *AJ*, 112, 1487
- Harris, W. E. 2010, ArXiv e-prints [arXiv:1012.3224]
- Helmi, A., Babusiaux, C., Koppelman, H. H., et al. 2018, *Nature*, 563, 85
- Helmi, A., White, S. D. M., de Zeeuw, P. T., & Zhao, H. 1999, *Nature*, 402, 53
- Hidalgo, S. L., Pietrinferni, A., Cassisi, S., et al. 2018, *ApJ*, 856, 125

- Horta, D., Lu, Y. L., Ness, M. K., Lisanti, M., & Price-Whelan, A. M. 2024, *ApJ*, 971, 170
- Horta, D., Schiavon, R. P., Mackereth, J. T., et al. 2020, *MNRAS*, 493, 3363
- Horta, D., Schiavon, R. P., Mackereth, J. T., et al. 2021, *MNRAS*, 500, 1385
- Ibata, R. A., Gilmore, G., & Irwin, M. J. 1994, *Nature*, 370, 194
- Jean-Baptiste, I., Di Matteo, P., Haywood, M., et al. 2017, *A&A*, 604, A106
- Khoperskov, S. & Gerhard, O. 2022, *A&A*, 663, A38
- Kirby, E. N., Cohen, J. G., Guhathakurta, P., et al. 2013, *ApJ*, 779, 102
- Koppelman, H. H., Bos, R. O. Y., & Helmi, A. 2020, *A&A*, 642, L18
- Koppelman, H. H., Helmi, A., Massari, D., Price-Whelan, A. M., & Starkenburg, T. K. 2019, *A&A*, 631, L9
- Kruijssen, J. M. D., Pfeffer, J. L., Chevance, M., et al. 2020, *MNRAS*, 498, 2472
- Kruijssen, J. M. D., Pfeffer, J. L., Reina-Campos, M., Crain, R. A., & Bastian, N. 2019, *MNRAS*, 486, 3180
- Lallement, R., Capitanio, L., Ruiz-Dern, L., et al. 2018, *A&A*, 616, A132
- Lane, J. M. M., Bovy, J., & Mackereth, J. T. 2023, *MNRAS*, 526, 1209
- Leaman, R., VandenBerg, D. A., & Mendel, J. T. 2013, *MNRAS*, 436, 122
- Majewski, S. R., Schiavon, R. P., Frinchaboy, P. M., et al. 2017, *AJ*, 154, 94
- Malhan, K., Ibata, R. A., Sharma, S., et al. 2022, *ApJ*, 926, 107
- Marín-Franch, A., Aparicio, A., Piotto, G., et al. 2009, *ApJ*, 694, 1498
- Massari, D., Aguado-Agelet, F., Monelli, M., et al. 2023, *A&A*, 680, A20
- Massari, D., Koppelman, H. H., & Helmi, A. 2019, *A&A*, 630, L4
- Mikkola, D., McMillan, P. J., & Hobbs, D. 2023, *MNRAS*, 519, 1989
- Milone, A. P., Piotto, G., Bedin, L. R., et al. 2012, *A&A*, 540, A16
- Milone, A. P., Piotto, G., Renzini, A., et al. 2017, *MNRAS*, 464, 3636
- Minelli, A., Mucciarelli, A., Massari, D., et al. 2021, *ApJ*, 918, L32
- Montalbán, J., Mackereth, J. T., Miglio, A., et al. 2021, *Nature Astronomy*, 5, 640
- Monty, S., Belokurov, V., Sanders, J. L., et al. 2024, *MNRAS*, 533, 2420
- Mori, A., Di Matteo, P., Salvadori, S., et al. 2024, *A&A*, 690, A136
- Myeong, G. C., Vasiliev, E., Iorio, G., Evans, N. W., & Belokurov, V. 2019, *MNRAS*, 488, 1235
- Naidu, R. P., Conroy, C., Bonaca, A., et al. 2020, *ApJ*, 901, 48
- Naidu, R. P., Conroy, C., Bonaca, A., et al. 2021, *ApJ*, 923, 92
- Nardiello, D., Libralato, M., Piotto, G., et al. 2018, *MNRAS*, 481, 3382
- Oria, P.-A., Tenachi, W., Ibata, R., et al. 2022, *ApJ*, 936, L3
- Orkney, M. D. A., Laporte, C. F. P., Grand, R. J. J., et al. 2022, *MNRAS*, 517, L138
- Pancino, E., Bellazzini, M., Giuffrida, G., & Marinoni, S. 2017, *MNRAS*, 467, 412
- Pietrinferni, A., Hidalgo, S., Cassisi, S., et al. 2021, *ApJ*, 908, 102
- Piotto, G., Milone, A. P., Bedin, L. R., et al. 2015, *AJ*, 149, 91
- Queiroz, A. B. A., Anders, F., Chiappini, C., et al. 2023, *A&A*, 673, A155
- Rey, M. P., Agertz, O., Starkenburg, T. K., et al. 2023, *MNRAS*, 521, 995
- Salaris, M., Chieffi, A., & Straniero, O. 1993, *ApJ*, 414, 580
- Sarajedini, A. & Demarque, P. 1990, *ApJ*, 365, 219
- Souza, S. O., Libralato, M., Nardiello, D., et al. 2024, *A&A*, 690, A37
- Stetson, P. B., Vandenberg, D. A., & Bolte, M. 1996, *PASP*, 108, 560
- VandenBerg, D. A., Brogaard, K., Leaman, R., & Casagrande, L. 2013, *ApJ*, 775, 134
- Vasiliev, E. & Baumgardt, H. 2021, *MNRAS*, 505, 5978
- Villalobos, Á. & Helmi, A. 2008, *MNRAS*, 391, 1806
- Walker, I. R., Mihos, J. C., & Hernquist, L. 1996, *ApJ*, 460, 121
- Xiang, M. & Rix, H.-W. 2022, *Nature*, 603, 599

## Appendix A: Isochrone fitting results

In this Appendix we show the results of our isochrone fitting algorithm applied to the 13 GCs under study in this work, with the exception of NGC 288 that is already shown in Fig. 1 in the main paper. Each figure is made up of four panels. The lower ones show the posterior distribution of the parameters of the model, including their correlation, resulting from the fit of the  $(m_{F814W}, m_{F606W}-m_{F814W})$  CMD and of the  $(m_{F606W}, m_{F606W}-m_{F814W})$  CMD. The upper panels show the isochrone corresponding to the best-fitting solution to the observed CMDs, where the green symbols mark the stars that were actually selected for the fit. We refer the reader to Paper I for further details about the method.

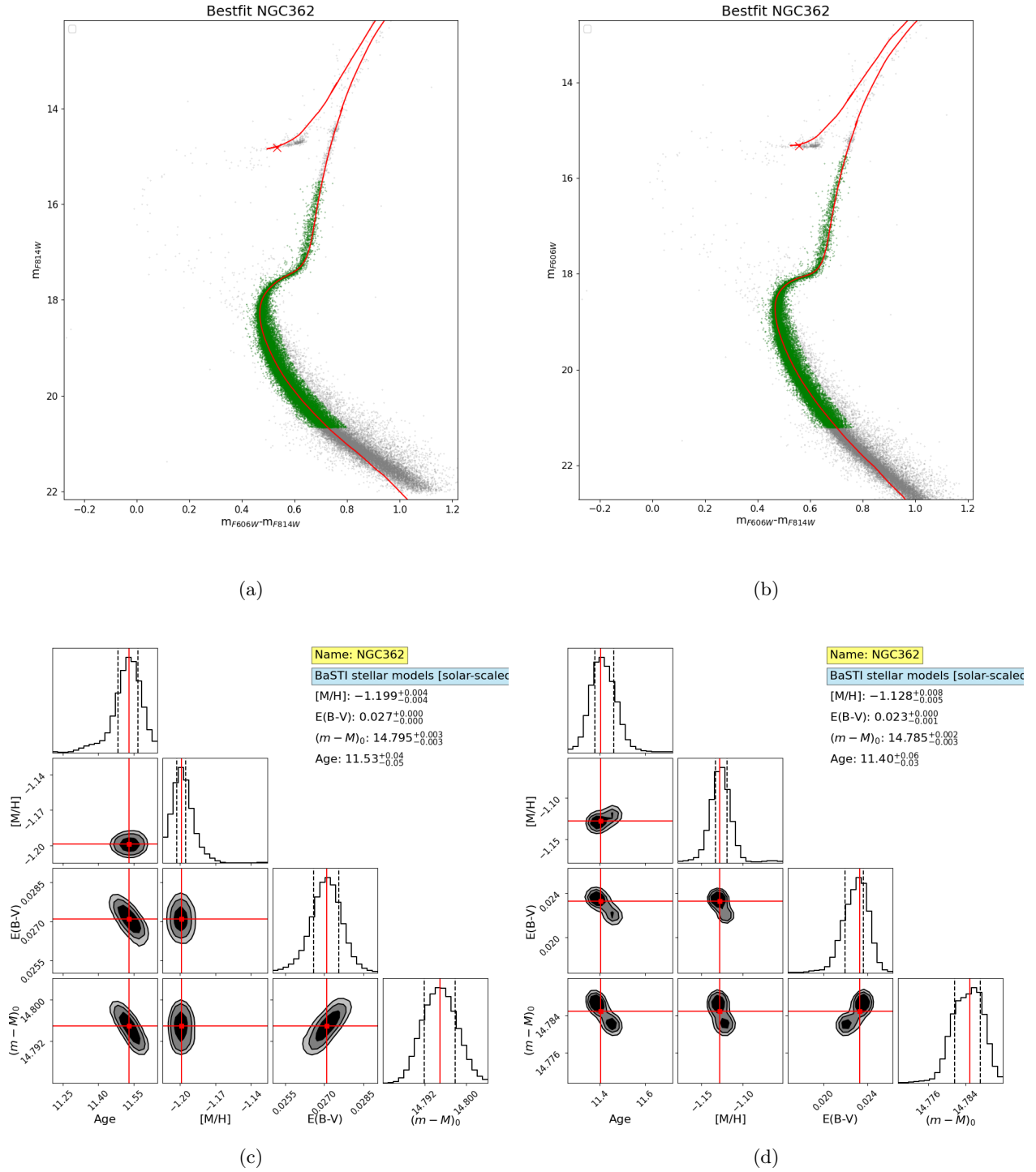


Fig. A.1: Results for NGC362. The meaning of the panels is the same as in Fig. A.1

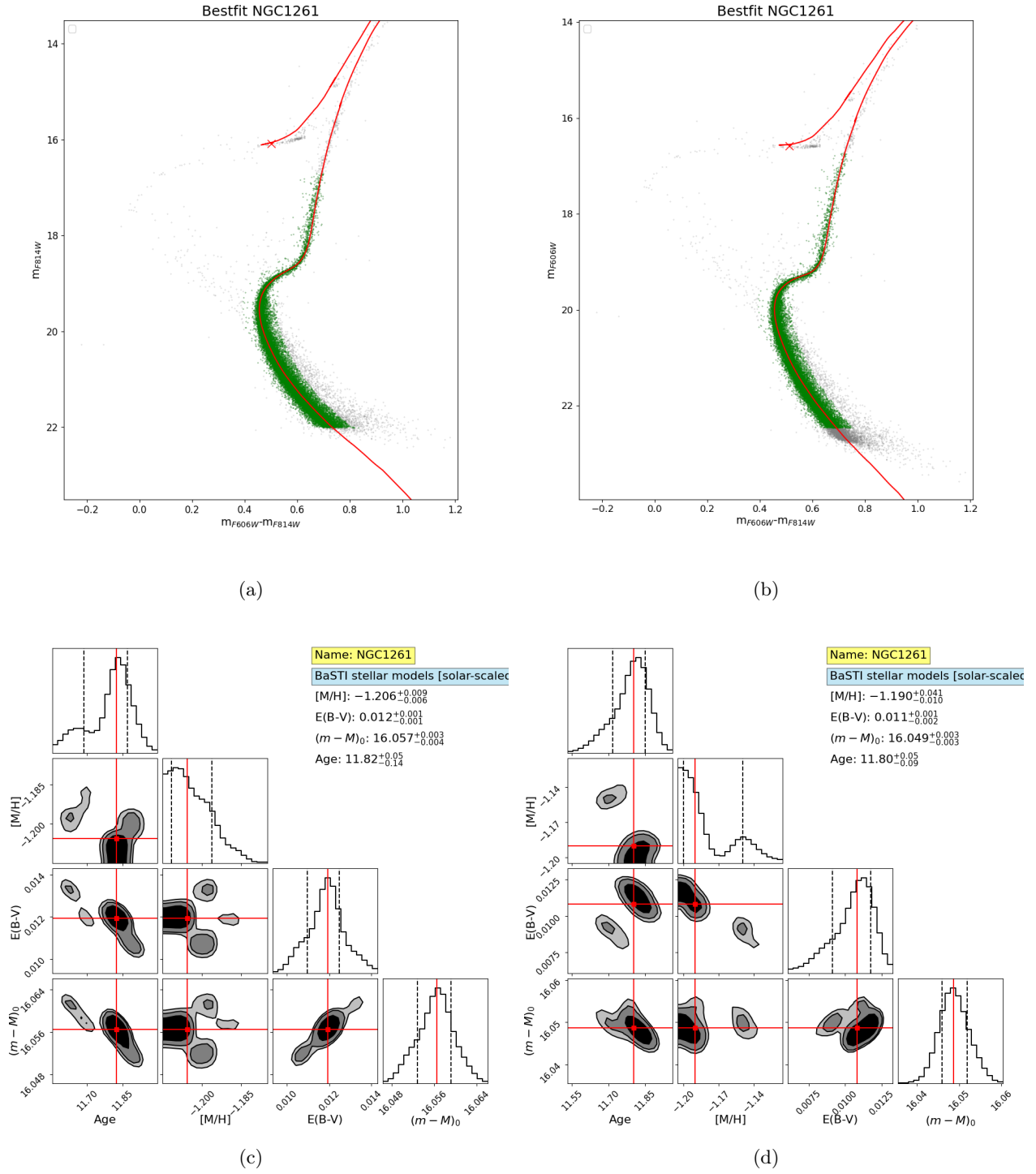


Fig. A.2: Results for NGC1261. The meaning of the panels is the same as in Fig. A.1

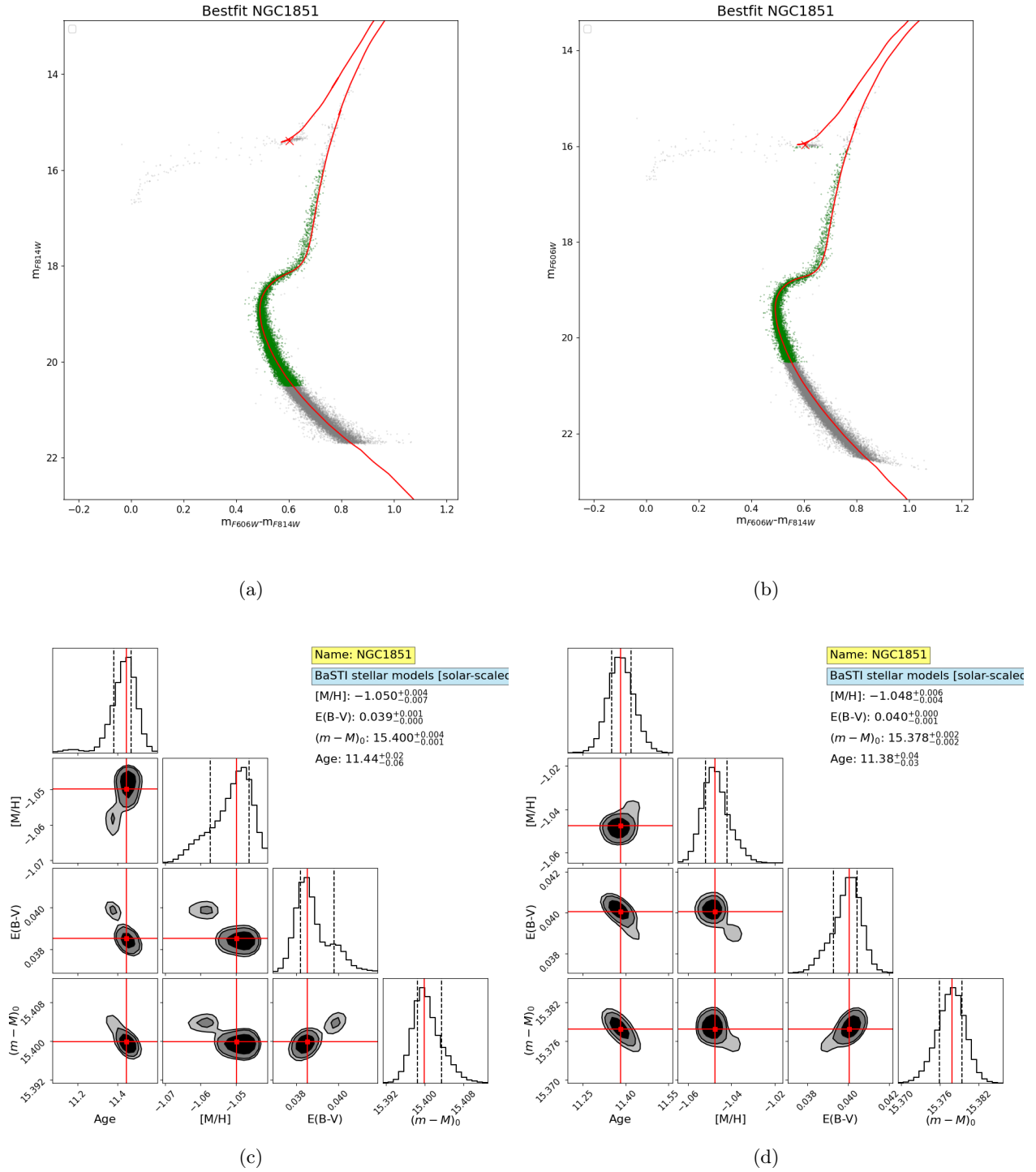


Fig. A.3: Results for NGC1851. The meaning of the panels is the same as in Fig. A.1

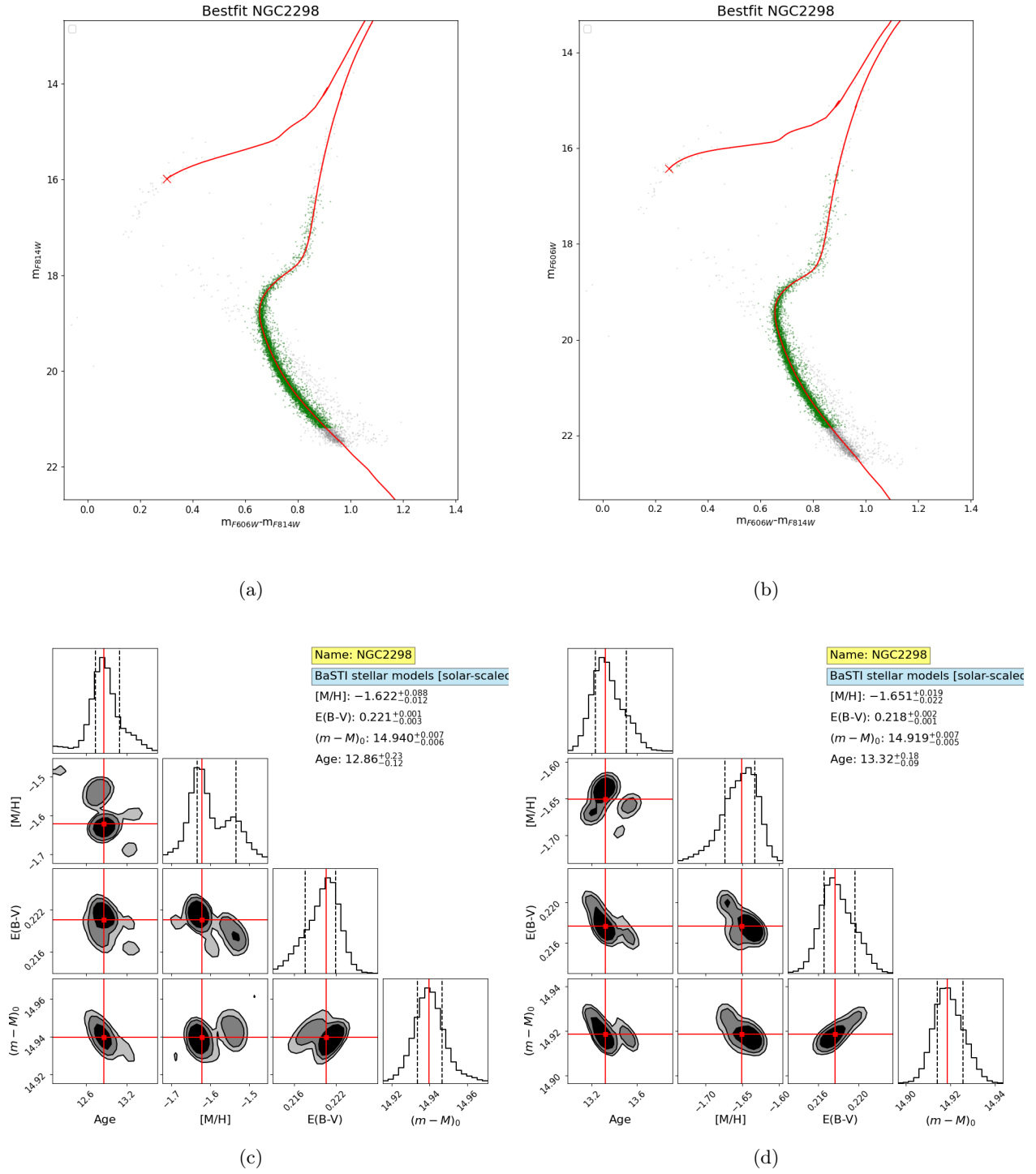


Fig. A.4: Results for NGC2298. The meaning of the panels is the same as in Fig. A.1

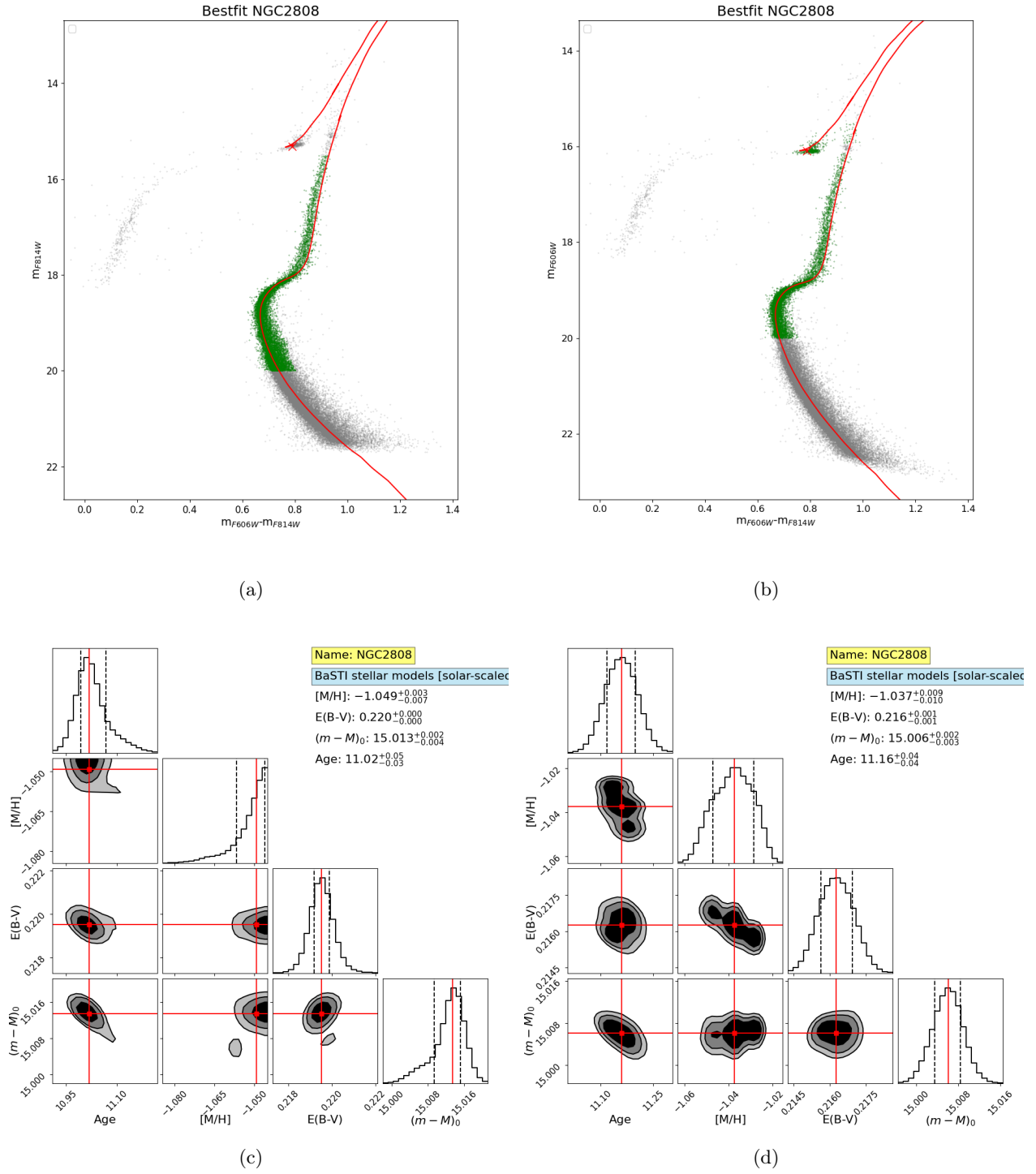


Fig. A.5: Results for NGC2808. The meaning of the panels is the same as in Fig. A.1



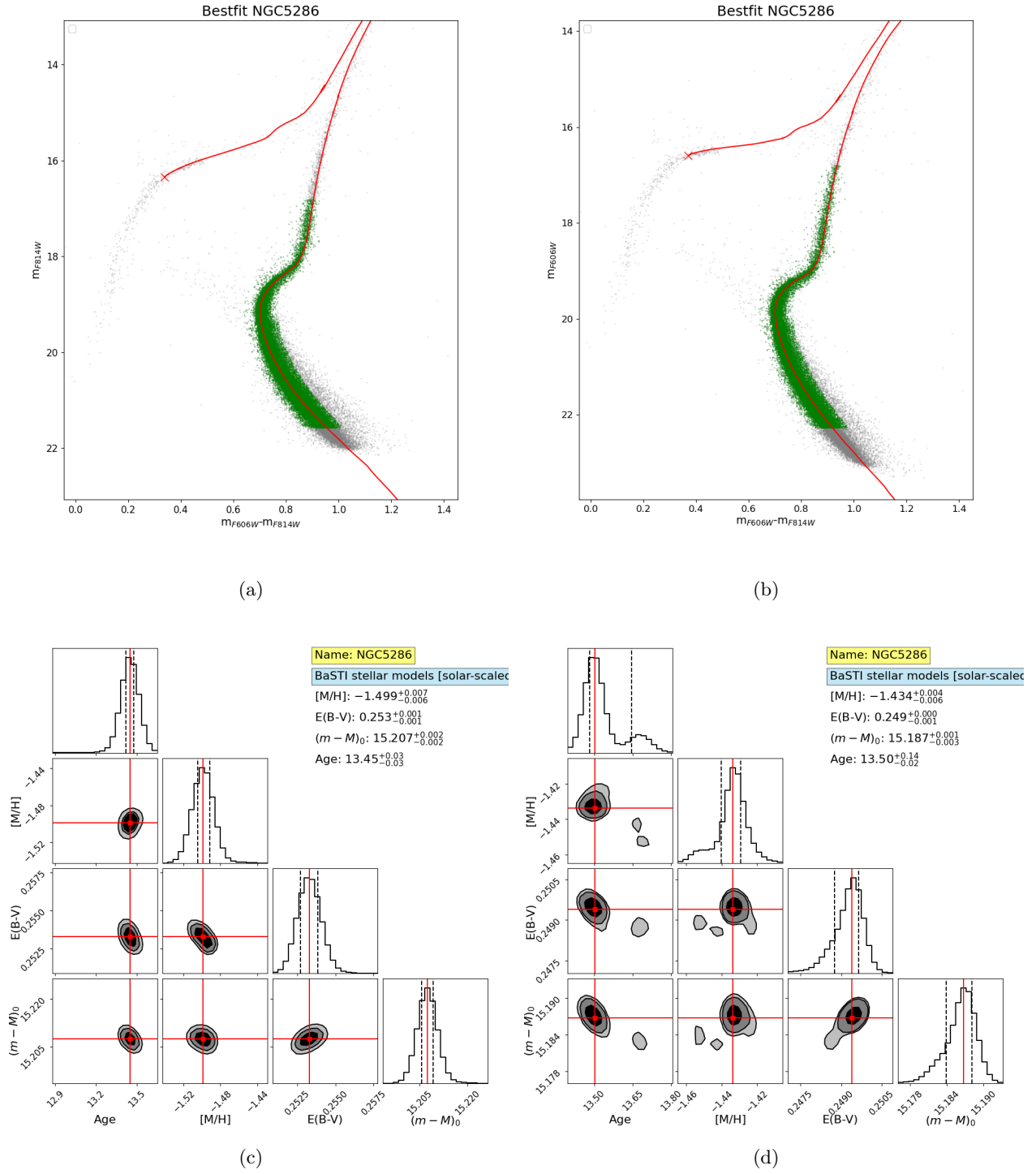


Fig. A.6: Results for NGC5286. The meaning of the panels is the same as in Fig. A.1

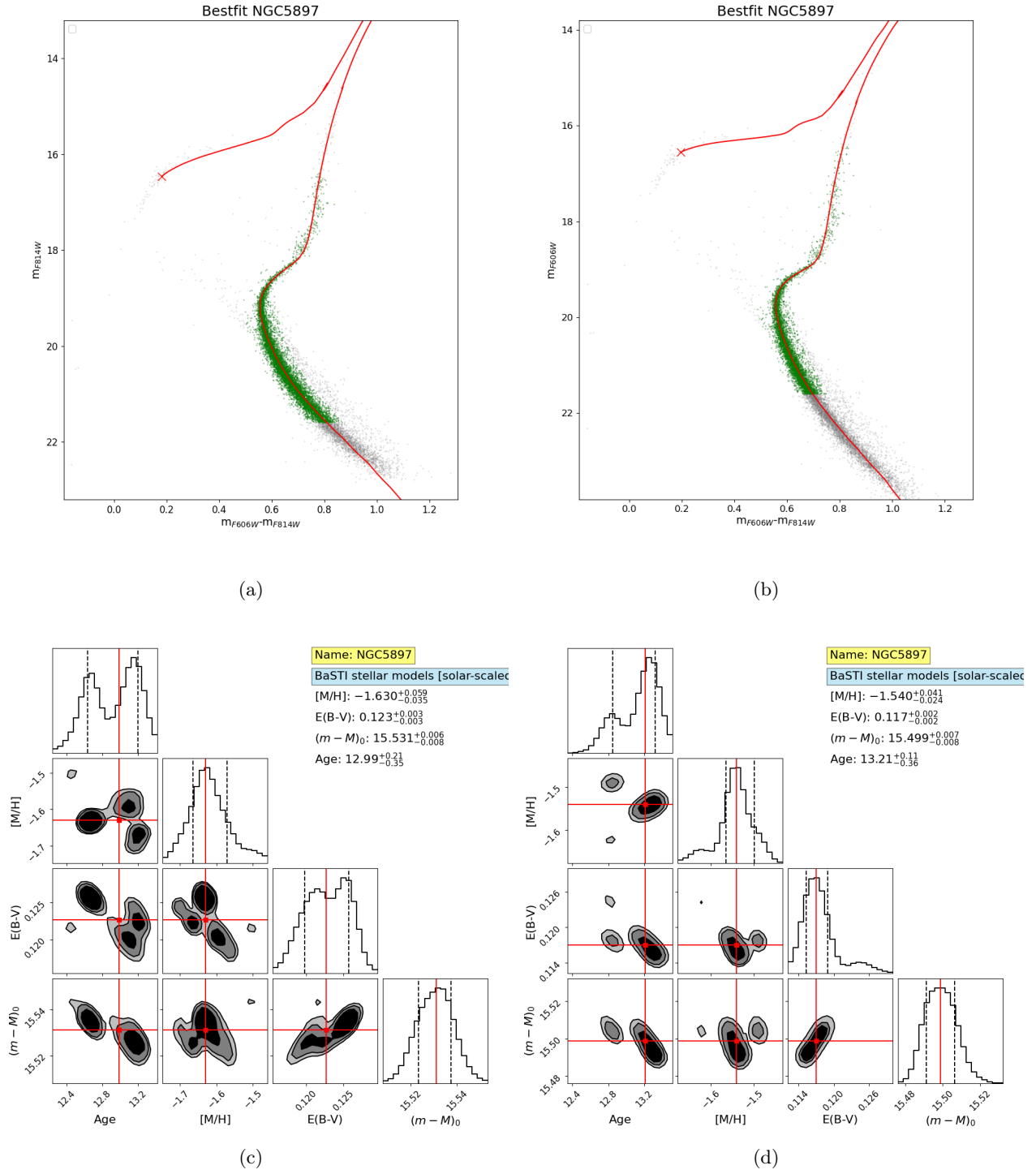


Fig. A.7: Results for NGC5897. The meaning of the panels is the same as in Fig. A.1

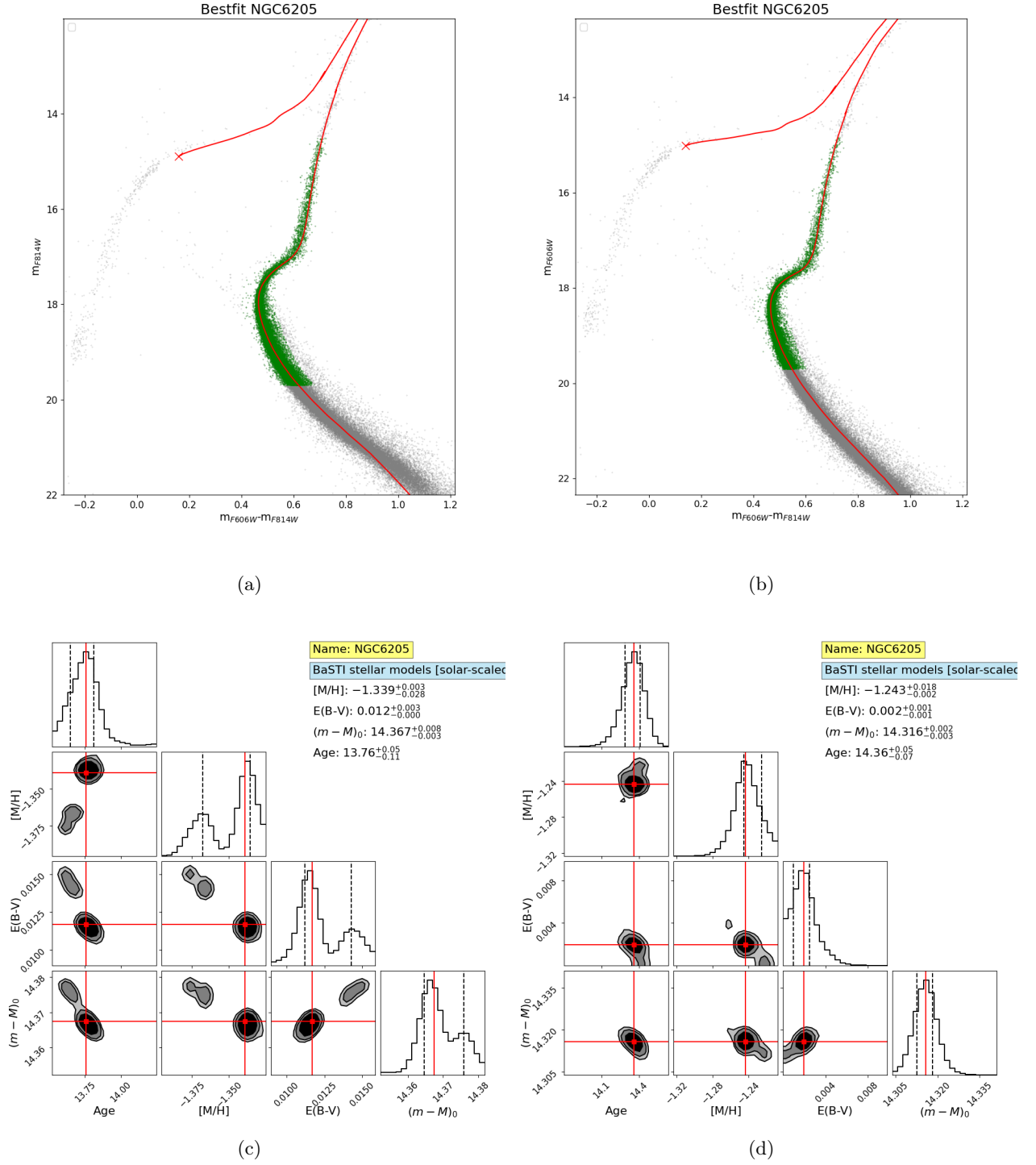


Fig. A.8: Results for NGC6205. The meaning of the panels is the same as in Fig. A.1

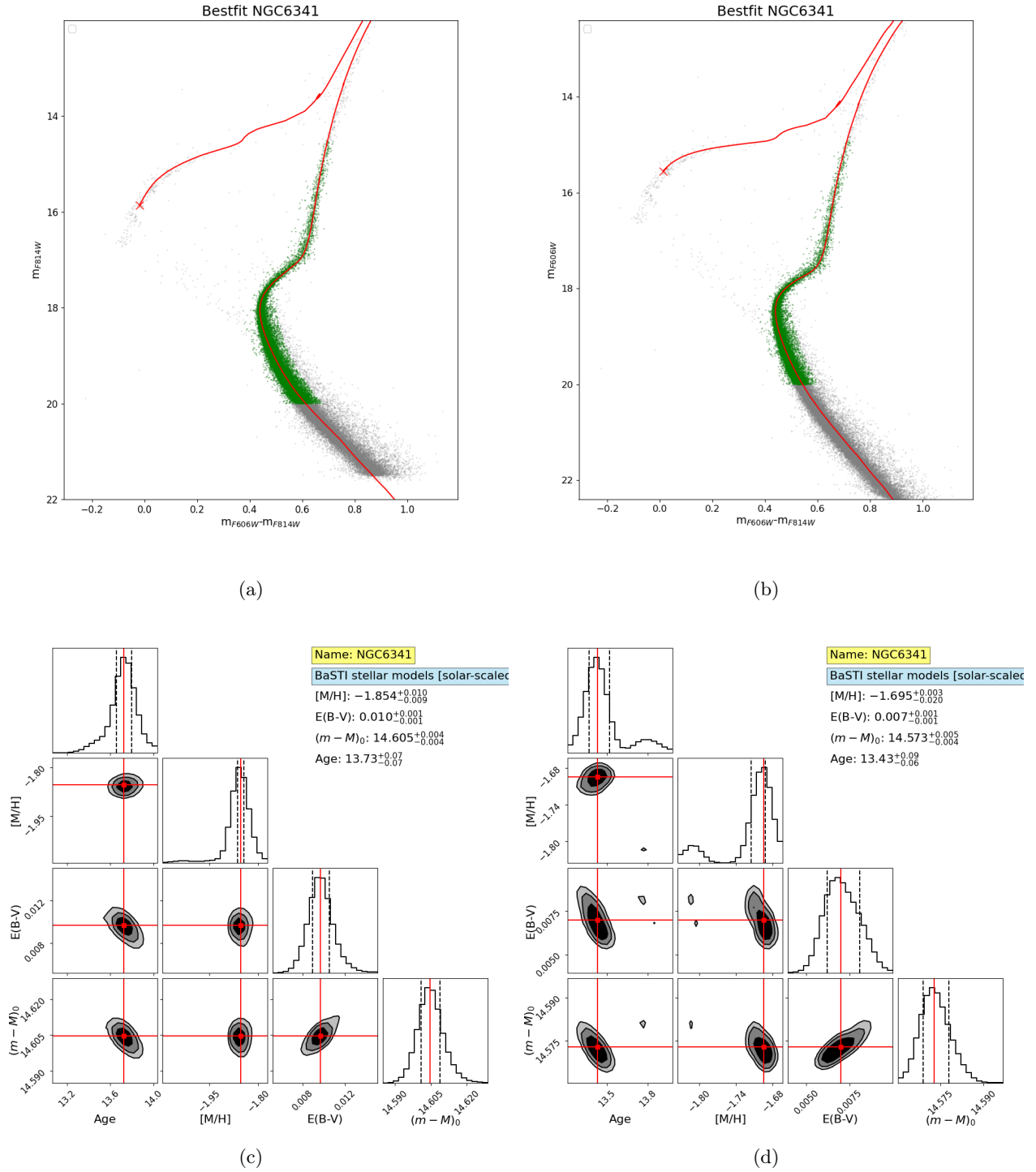


Fig. A.9: Results for NGC6341. The meaning of the panels is the same as in Fig. A.1

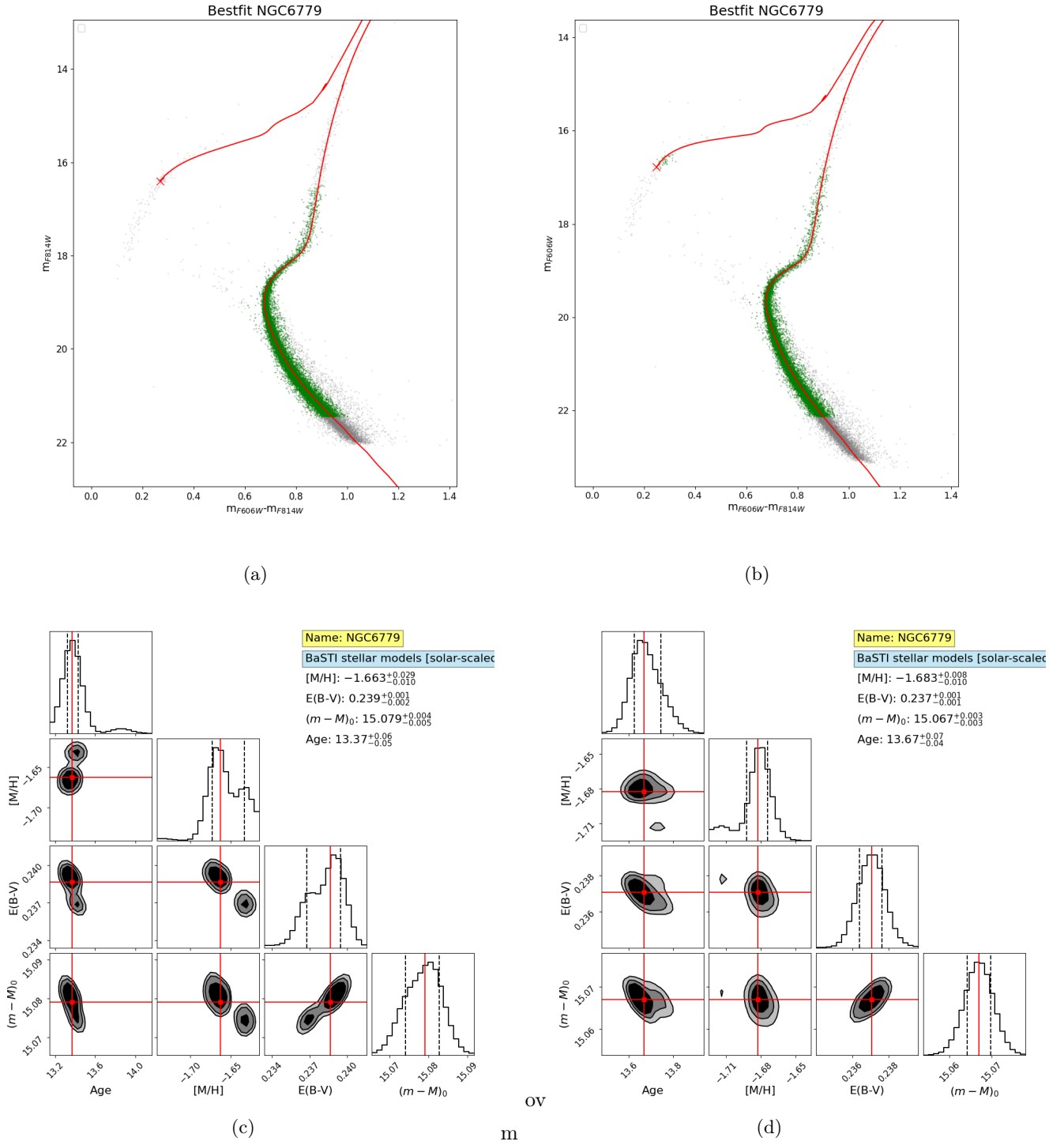


Fig. A.10: Results for NGC6779. The meaning of the panels is the same as in Fig. A.1

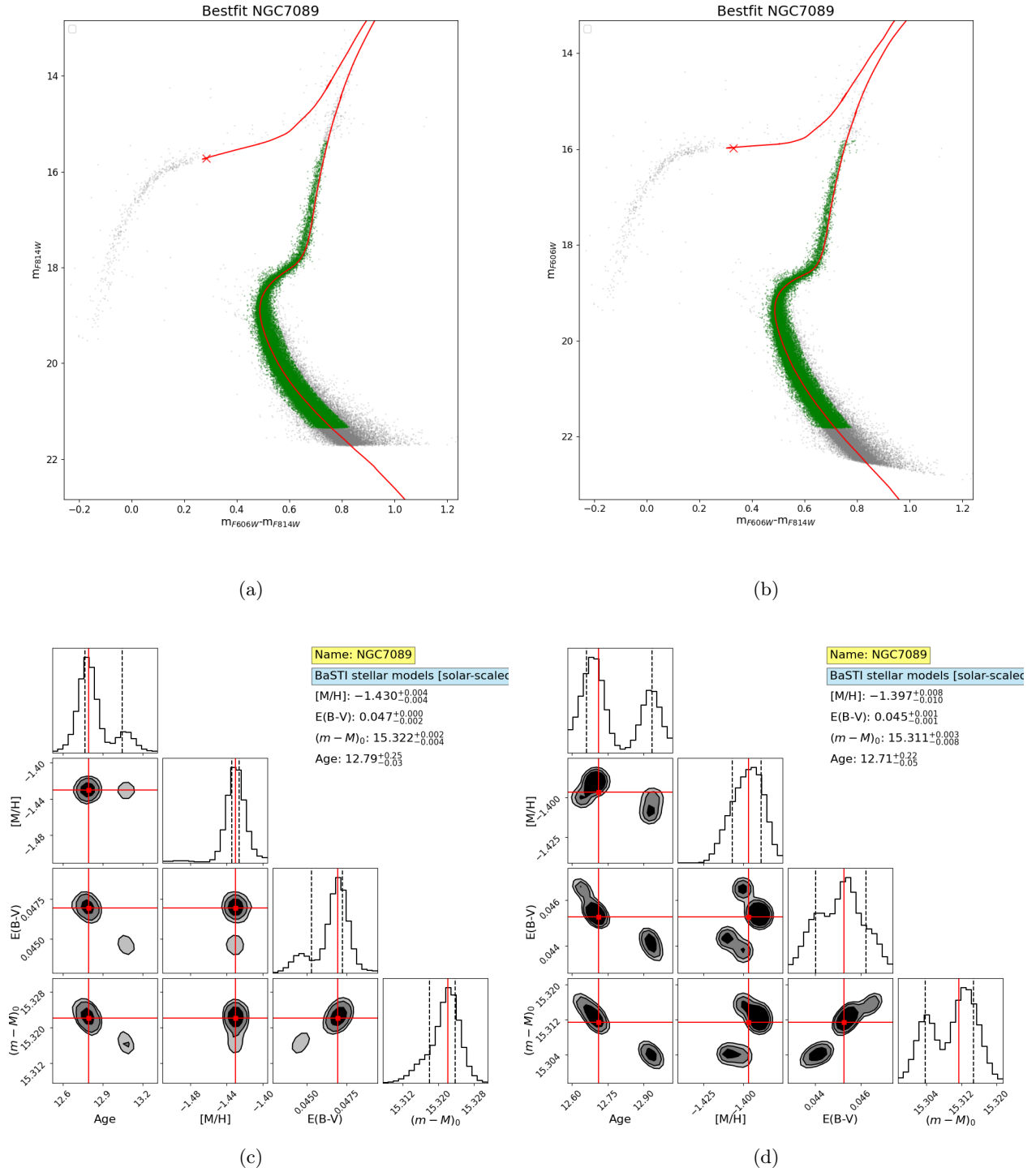


Fig. A.11: Results for NGC7089. The meaning of the panels is the same as in Fig. A.1

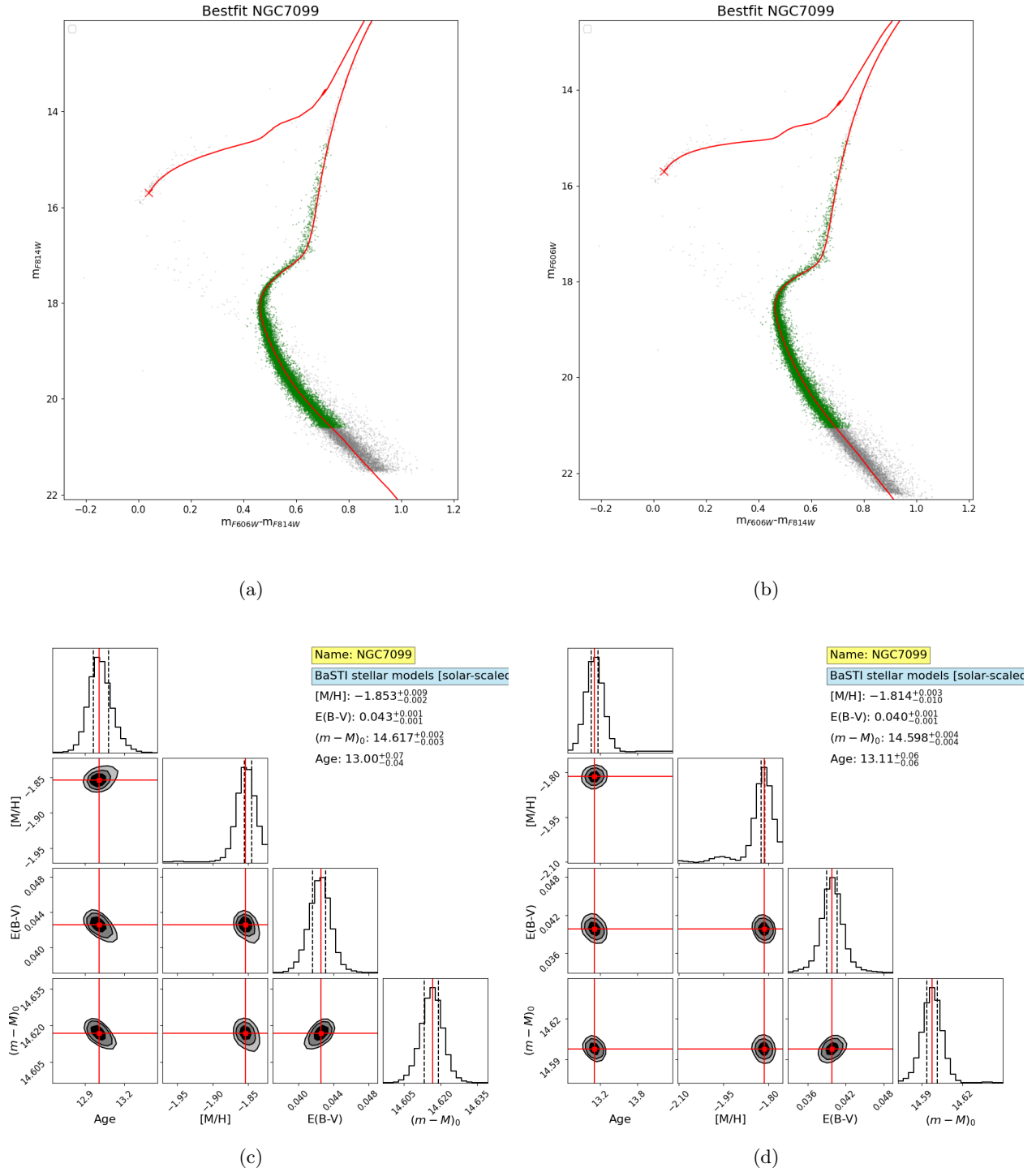


Fig. A.12: Results for NGC7099. The meaning of the panels is the same as in Fig. A.1